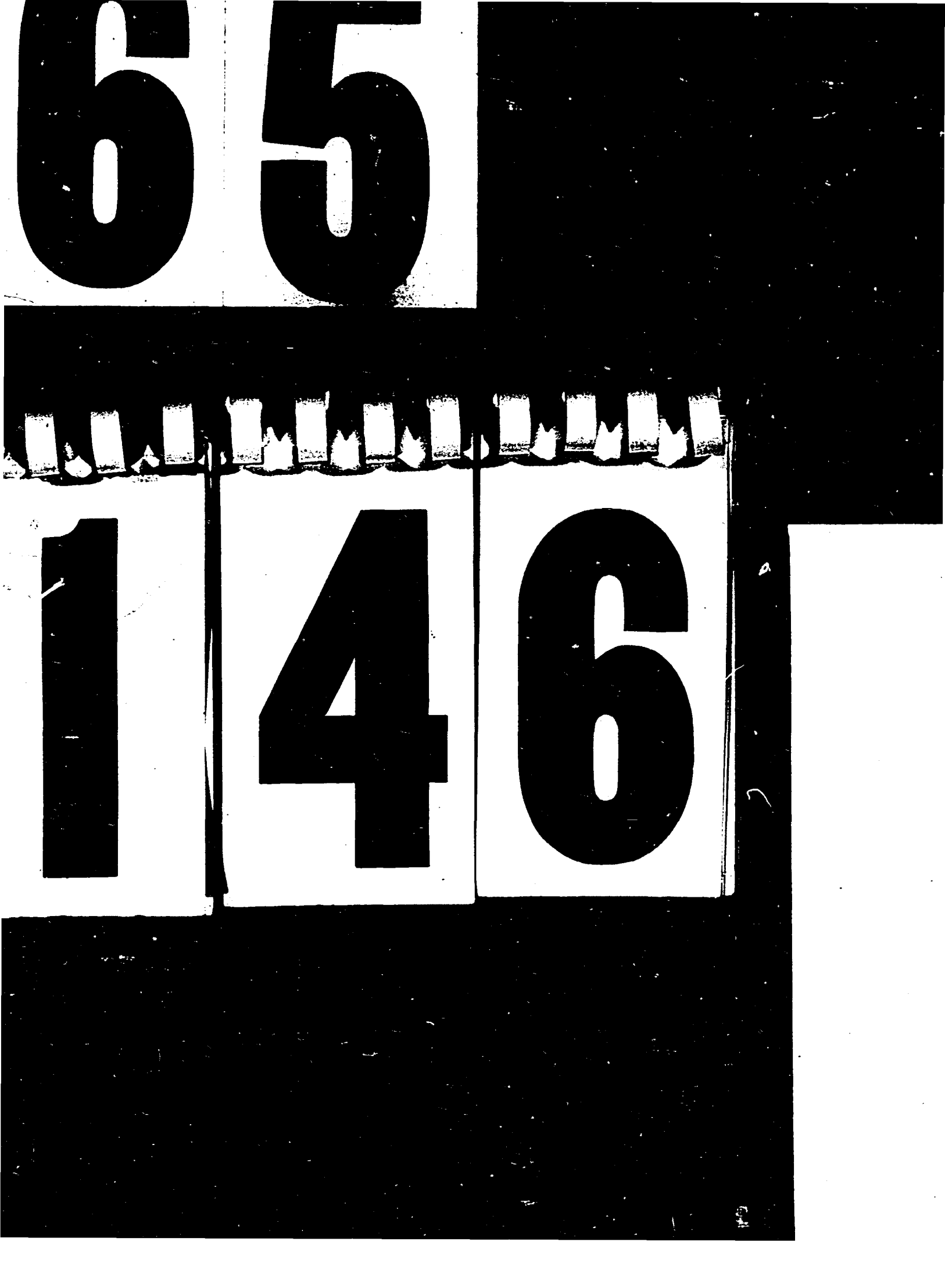
65
146

THE UNIVERSITY OF OKLAHOMA

GRADUATE COLLEGE

THE INVESTIGATION OF ION VELOCITY IN ELECTRICAL PREBREAKDOWN USING MICROWAVE DOPPLER REFLECTOMETER TECHNIQUE

A DISSERTATION

SUBMITTED TO THE GRADUATE FACULTY

in partial fulfillment of the requirement for the

degree of

DOCTOR OF PHILOSOPHY

BY

HUEI LING

Norman, Oklahoma

1965

THE INVESTIGATION OF ION VELOCITY IN ELECTRICAL PREBREAKDOWN

USING MICROWAVE DOPPLER REFLECTOMETER TECHNIQUE

APPROVED BY

DISSERTATION COMMITTEE

ACKNOWLEDGEMENT

The author's deep feeling of gratitude toward Dr. James D. Palmer can not be aptly expressed. Dr. Palmer's patient advice, help and encouragement during the course of this research has been sincerely appreciated and will not be forgotten.

The author is grateful to the University of Oklahoma for financial support by means of a graduate assistantship during the academic year 1962-1964.

TABLE OF CONTENTS

LIST OF TABLES

LIST OF ILLUSTRATIONS

THE INVESTIGATION OF ION VELOCITY IN ELECTRICAL PREBREAKDOWN USING MICROWAVE DOPPLER REFLECTOMETER TECHNIQUE

CHAPTER I

INTRODUCTION

One measure that has eluded researchers in the field of preignition studies of gas discharge throughout many years of research has been the direct measurement of positive ion velocity in electrical prebreakdown. This parameter has remained unsolved, although thoroughly researched over a period of many years. Early work in the field of ionization and breakdown was carried on by Townsend (37) and other workers (30,31). In honor of Townsend's work, this type of discharge was named the Townsend Discharge.

Townsend attempted to measure ion velocity at low pressure in 1914 (36), however, it was found later that his method was not applicable to ionic speed, although he was able to measure electron mobility.

Since the work down by Townsend, the more recent work in the measurement of gas discharge properties has been by Von Engel (39), by Loeb (17), Loeb and Meek (19), Raether (16), and many others (44, 29). Methods of observation have ranged from Cloud Chamber

detection used by Raether to oscilloscope waveforms reported by Von Engel and through photomultiplier detectors looking at the luminous streamer front used by Loeb and by Loeb and Meek. None of these has been successful in measuring the average velocity of the positive ion front as it approaches the cathode.

Under normal conditions gases show little conductivity. The conductivity is produced by the external agencies, such as electric field, cosmic rays, γ-radiations and radioactive traces from container walls. Use of any of the many agencies which cause liberation of electrons and/or ions from surfaces or liberate electrons from atoms and molecules of the gas can augment the ionizing events.

Attempts to derive a simple expression for the velocity of ions as a function of the reduced electric field have resulted in expressions which differ widely from experimental data (9). The reason is that an ion, being relatively slow, stays in the vicinity of gas molecules long enough to polarize them. The resultant attractive force not only shortens the mean free path of the ion, but also causes a continuous exchange of momentum which appreciably reduces the drift velocity. Furthermore, the size of the ion and charge transfer play important roles; the latter especially when ions move in their own gas.

Due to the lack of a unique method for measuring the ion velocity, the fundamental processes involved in electrical prebreakdown phenomena remain a debatable topic. For example, under low pressure, the spark flash has the form of a wide glow (8) for which the Townsend and Von Engel theories seem to agree quite well. However, under high pressure the flash is narrow and in the form of a luminous streak which can not

be explained by the Townsend or Von Engel theories, but is explained adequately by the canal or streamer (8, 16) theory of Loeb and Meek.

The interest in guided waves in velocity measurement dates back to the time of World War II. Soon after the war was over, the highly developed microwave techniques were applied to experimental studies of gaseous discharges (42). Experiments have been made in which the effect of ionized gas on the propagation of low power microwave signals has been measured by Varnerin (38). The phase shift caused by the refractive index of the medium can be measured by microwave interometer techniques which has been done by Goldstein (12), Anderson (1), Whitmer (41), Wharton (40), Brown (5), Postma (36), Buser (6), and Drummond (7). None of the techniques used by these researchers have been able to measure the velocity of the ions at onset. Doppler reflectometer as a technique for measuring the ion velocity in preignition breakdown is an entirely new use of this particular method.

The present program has thus evolved from a desire to develop an experimental technique as well as a theoretical derivation which would enable measurement of the velocity of ions in electrical prebreakdown. Use has been made of the Doppler reflectometer concept i.e. propagating into a stationary medium, pulsing the medium during rf burst and looking at propagation of the wavefront of positive ions, whether toward or away from the electrode through which the horn of the reflectometer is pointing.

The experimental results show, for example, at a carrier frequency of 33.55 kmc, the Doppler shift was 4/46 megacycles giving a velocity

of 0.38×10^3 meters per second. It is hoped that this study will contribute some knowledge of ion speed which would be valuable in the study of fundamental processes in gaseous electrical breakdown.

CHAPTER II

REVIEW OF THE PREVIOUS WORK AND THE OBJECTIVES

Previous Investigations (23)

The investigation of properties of gaseous electrical discharge has experienced a rapid expansion in recent years, particularly electromagnetic field interaction with plasma. Technical journals in physics and electrical engineering have devoted special issues to this subject.

In spite of the great amount of work being done, very little effort has been placed on determining ion velocities in gaseous discharge.

Typical of the work in this field are the investigations of Townsend (36), Von Engel (39), Loeb (17) and Meek (20) which will be examined in detail.

The Townsend Theory (37)

Assume electrons will be emitted by injecting an $h\upsilon$ to the cathode as shown in Figure 1.

Let α represent the number of ion pairs per meter formed by an electron moving toward the anode and dn be the number of ion formed per second in a slab at x of unit cross section and thickness dx. Then, the number of new electrons formed by n electrons traveling a distance dx is

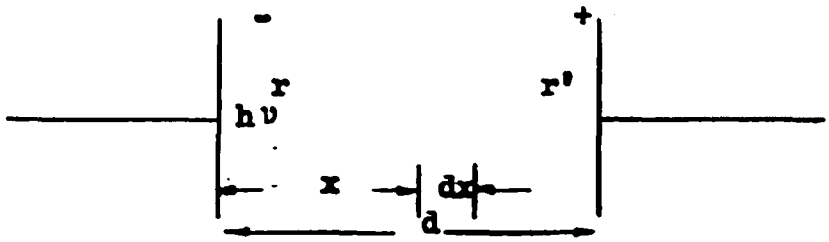

Figure 1

$$dn = n\alpha dx$$

$$n = Ae^{\alpha x}$$

Initial conditions:

$$x = 0 \qquad n = n_o$$

$$A = n_o$$

$$n = n_o e^{\alpha d}$$

$$i = i_o e^{\alpha d}$$

$$\frac{i}{i_o} = e^{\alpha d}$$

$$\ln \frac{i}{i_o} = \alpha d$$

$$d = \frac{1}{\alpha} \ln \frac{i}{i_o}$$

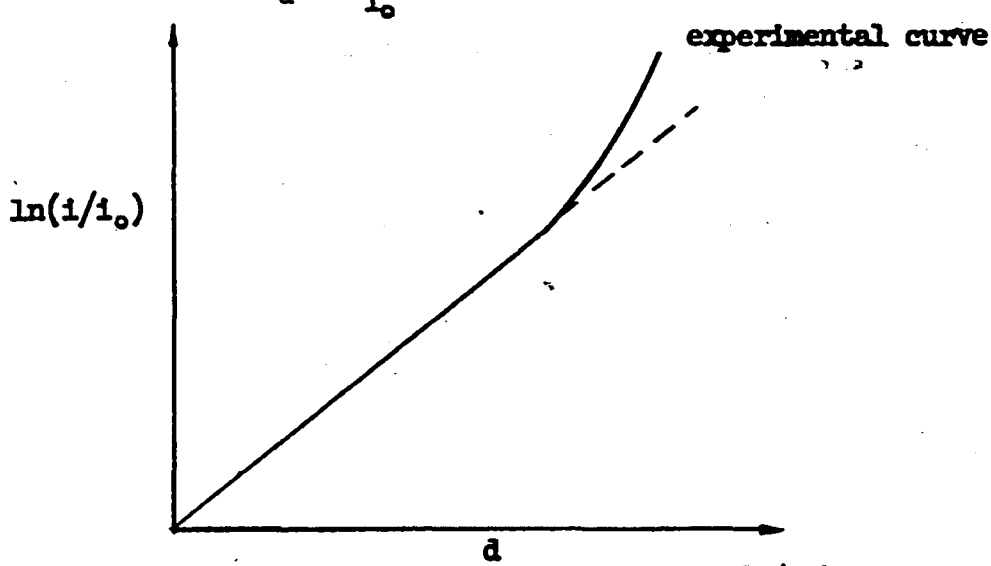

Figure 2 Plot of d Versus $\ln(i/i_o)$

However, experimental data do not agree with the derived equations.

Townsend assumed that each positive ion made β ionizing collisions in advancing a unit distance.

If n_o is the number of negative ions from the cathode, then $n_o e^{\alpha d}$ will reach the anode. Therefore, $n_o(e^{\alpha d} - 1)$ positive ions are produced in the gas and move in the opposite direction.

If n is the total number of negative ions that reach the anode, then $(n - n_o)$ will be the number of ions generated in the gas.

According to Figure 1

Let r be produced in x

r' be produced in (d-x)

$n = n_o + r + r'$

α be the number of ions produced by a negative ion.

β be the number of ions produced by a positive ion. (both in unit area)

The number of ions dr, generated between the two planes at distance x and x + dx is

$$dr = (n_o + r)dx + \beta r'dx$$

$$\frac{dr}{dx} = (n_o + r) + \beta r'$$

$$r' = n - n_o - r$$

$$\frac{dr}{dx} = \alpha (n_o + r) + \beta (n - n_o - r)$$

$$= (\alpha - \beta)(n_o + r) + \beta n$$

$$\frac{dr}{dx} - (\alpha - \beta)(n_o + r) - \beta n = 0$$

Using the integrating factor $e^{-\int(\alpha - \beta)dx} = e^{-(\alpha - \beta)x}$

$$e^{-(\alpha-\beta)x}\frac{dr}{dx} - (\alpha-\beta)(n_o + r)e^{-(\alpha-\beta)x} - \beta n e^{-(\alpha-\beta)x} = 0$$

$$\frac{d}{dx} e^{-(\alpha-\beta)x}(n_o + r) = \beta e^{-(\alpha-\beta)x}$$

$$e^{-(\alpha-\beta)x}(n_o + r) = -\frac{\beta}{(\alpha-\beta)} n e^{-(\alpha-\beta)x} + c$$

$$n_o + r = -\frac{\beta n}{(\alpha-\beta)} + ce^{(\alpha-\beta)x}$$

where $r = 0;\ x = 0$

$$c = n_o + \frac{\beta n}{\alpha-\beta}$$

$$(n_o + r)e^{-(\alpha-\beta)x} = -\frac{\beta n}{\alpha-\beta} e^{-(\alpha-\beta)x} + \left(n_o + \frac{\beta n}{\alpha-\beta}\right)$$

$$n_o + r = -\frac{\beta n}{\alpha-\beta} + \left(n_o + \frac{\beta n}{\alpha-\beta}\right)e^{(\alpha-\beta)x}$$

when $x = d;\ r = n - n_o\ ;\ n_o + r = n$

$$n = -\frac{\beta n}{\alpha-\beta} + n_o + \frac{\beta n}{\alpha-\beta} e^{(\alpha-\beta)d}$$

$$n - \frac{\beta n}{\alpha-\beta} e^{(\alpha-\beta)d} + \frac{\beta n}{\alpha-\beta} = n_o e^{(\alpha-\beta)d}$$

$$n\left[\alpha - \beta - \beta e^{(\alpha-\beta)d} + \beta\right] = n_o(\alpha-\beta)e^{(\alpha-\beta)d}$$

$$n = n_o \frac{(\alpha-\beta)e^{(\alpha-\beta)d}}{\alpha - \beta e^{(\alpha-\beta)d}}$$

or

$$i = i_o \frac{(\alpha-\beta)e^{(\alpha-\beta)d}}{\alpha - \beta e^{(\alpha-\beta)d}}$$

This equation is accurate in determining discharge currents under certain conditions. These conditions are that the pressure times distance (pd) product be a small number, that the ratio of applied electric field to gap pressure (E/p) be relatively small, and the total time for the discharge to form and dissipate most of its energy be more than 10^{-5} seconds. In general the theory holds for pd $\leq$ (1 cm) (1 atmosphere) for (E/p) $\leq$ 41.6 and for times not shorter than that required for the positive ions to cross the gap which is assumed to be approximately 10^{-5} seconds for a one centimeter gap.

The reasoning behind this limitation of the Townsend Theory is that the first Townsend coefficient α, is based on primary electron multiplication only, and the second is based on the release of secondary electrons from the cathode. The second coefficient, β , is the only one concerned with secondary effects and it has been shown that at least one other secondary mechanism must take place in discharges other than those described above to account for the time required for the discharge to be completed. For this reason one must look for other secondary effects which will account for the energy dissipation in the observed times in these discharges.

The Von Engel Theory (39)

The inadequate part of the Townsend equation is due to neglecting the auxiliary ionization, i.e., the secondary emission from the cathode.

Let n_p be the number of primary electrons emitted per unit area owing to the action of the external drift source on the cathode. If n_s is the number of secondary electrons emitted per unit area owing to any of the secondary ionizing processes at cathode, then, the total

number emitted is

$$n_o = n_p + n_s$$

$$n = n_o e^{\alpha x}$$

$$n_d = n_o e^{\alpha d}$$

But n_o of these come directly from the cathode; hence, the number of new ion pairs generated in the gas is

$$n_d - n_o = n_o (e^{\alpha d} - 1)$$

Let r stand for the average number of secondary electrons emitted from the cathode for each new positive ion formed in the gas. Thus, the total number of secondaries formed on unit area of the cathode per second is

$$n_s = r n_o (e^{\alpha d} - 1)$$

$$n_o = n_s + n_p$$

$$n_o = n_p + r n_o (e^{\alpha d} - 1)$$

$$n_o = \frac{n_p}{1 + r - re^{\alpha d}}$$

$$n = n_o e^{\alpha x}$$

$$n = \frac{n_p e^{\alpha x}}{1 + r - re^{\alpha d}}$$

$$n_d = \frac{n_p e^{\alpha d}}{1 + r - re^{\alpha d}}$$

or

$$i = i_o \frac{e^{\alpha d}}{1 + r - re^{\alpha d}}$$

When the denominator becomes zero or,

$$1 = r(e^{\alpha d} - 1)$$

the breakdown occurs, the higher the gas pressure the faster the criteria reach instability.

It should be noted that the multiplication process itself does not become unstable, but the results of it cause instability. As the pressure of the gas is increased the process of instability is speeded up, which requires a further development because the times involved are less than the times for an electron to cross the gap. The phenomenon of breakdown is explained in the following manner. The electrons leave the space charge region at a high rate leaving only positive ions. These positive ions give rise to their own local field (radial) which gives rise to further secondary effects with regard to excited atoms and neutrals. These secondary effects in the presence of local fields in the space charge region then contribute to the overall effect of breakdown in that they supply the necessary particales close enough to the electrode to account for the small times involved compared to the transit time across the gap. Thus, the breakdown of gases in the presence of electric fields is seen to be dependent upon the secondary effects and upon the space charge distortion of the field.

This distortion gives rise to the emission of additional secondary effects which account for the apparent decrease in transit time

of electrons across the interelectrode space. The breakdown which occurs by this process is generally self-sustaining in that no additional energy is required to keep the process going.

Once the breakdown has started, the attendant spark will follow the space charge distorted fields. This will account for the erratic path taken by the spark. Thus, in breakdown the multiplication and propagation processes take place in the direction of the local fields, which provides the necessary explaination for breakdown in gases in which the field to pressure ratio is large or the product pd is large. If a plot of the breakdown cycle is made, the effect of secondary processes is clearly shown. A typical breakdown characteristic is shown in Figure 3

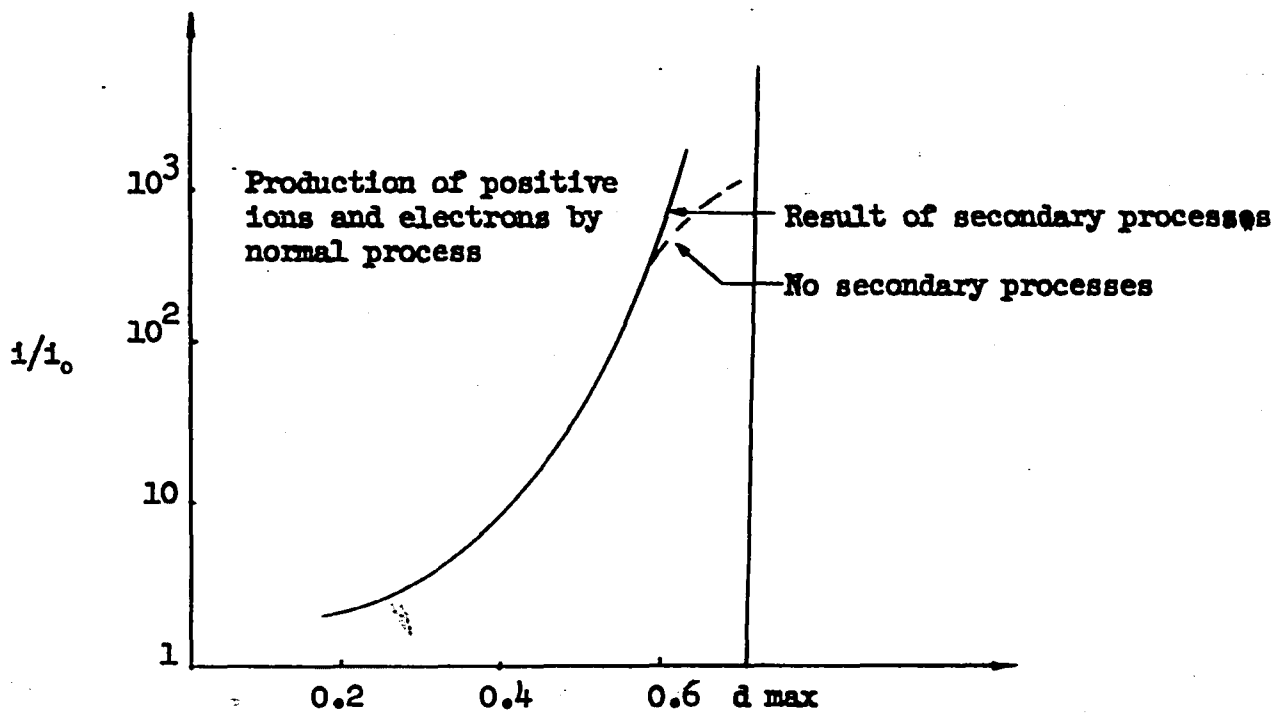

Figure 3 Breakdown Characteristic in a Uniform Field E

The most important features of this breakdown process are, first, that time per se does not enter in the process, and second, that the prime factor is the effect of secondary processes such as atoms in excited states and acceleration by local radial fields.

If a plot of voltage as a function of time is made from recorded data on breakdown, it can be seen that the total time for breakdown is approximately 10^{-8} seconds. This plot is shown in Figure 4.

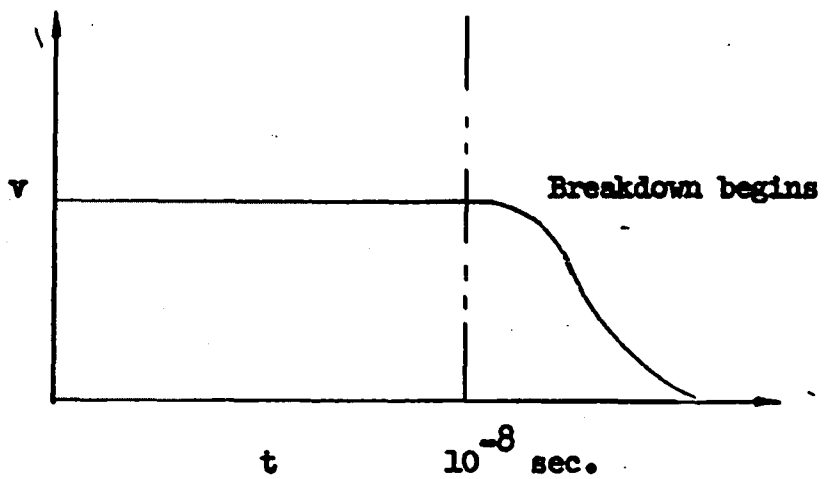

Figure 4 Breakdown Voltage as a Function of Time

The time required for an ion to travel from the anode to the cathode is of the order of 10^{-5} seconds, although no final solution exists to this problem. The essential point, however, is that at high pressure (1 atmosphere) the process is speeded up thereby causing instabilities. When the process is speeded up the electrons cannot leave the cathode at a sufficiently high rate to provide the necessary current carriers. Since this is the case other processes of creating electrons are necessary. According to Von Engel, the electrons leave first, and the positive ions left behind give rise to their own field which is radial as shown in Figure 5.

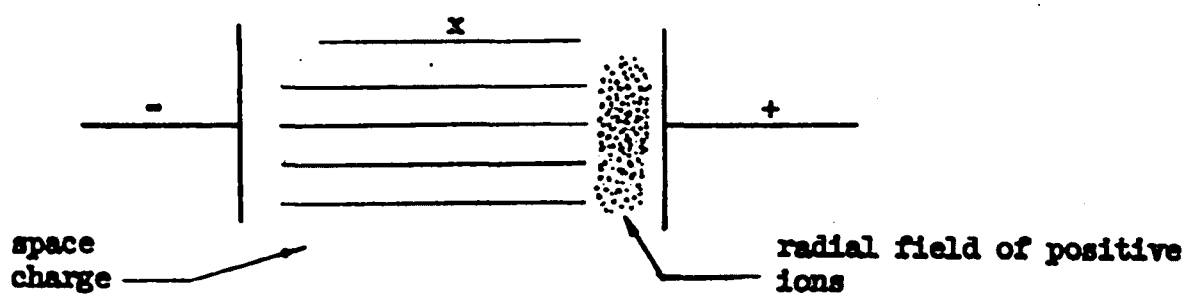

Figure 5

The local field then distorts the space charge fields which gives rise to the erratic course of the discharge as mentioned previously.

The Streamer Theory (20)

As measured by White and Raether the drift velocity of an electron is about 1.5 to 2 x 10^7 cm/sec., and the positive ion mobility is of the order of 10^{-2} to 10^{-4} that of electron.

As the electron avalanche advances, the rate of diffusion has been experimentally measured by Raether as

$$\bar{r} = 2Dt$$

Where $t = x/v$ is the time of advance of the avalanche and D is the diffusion coefficient.

Assuming that the ions are largely in a sphere of radius r, then, the field E_1 due to this space charge is

$$E_1 = \frac{4\pi qe}{4\pi r^2}$$

where e is the electron charge

q is the number of charges in the sphere

$$q = \frac{4}{3}\pi r^3 N$$

where N is the ion density

$$\therefore E_1 = \frac{4}{3} \pi r N e$$

For a distance dx at the end of a path, the number of ions resulting from the cumulative ionization is $e^{\alpha x} dx$. Thus

$$N = \frac{e^{\alpha x} dx}{\pi r^2 dx} = \frac{\alpha e^{\alpha x}}{\pi r^2}$$

r is the value of $\bar{r}$ caused by electron diffusion in crossing the gap.

$$\bar{r} = \sqrt{2Dt}$$

$$E_1 = \frac{4e\alpha e^{\alpha x}}{3\sqrt{2Dt}} = \frac{4e\alpha e^{\alpha x}}{3\sqrt{2D(x/v)}}$$

where v is the electron velocity

$$E_1 = \frac{4e\alpha e^{\alpha x}}{3\sqrt{(\frac{2D}{k})(\frac{x}{E})}}$$

k is the mobility. For example, a rough calculation of r as observed by Raether shows r = 0.013 cm, which makes E_1 = 6000 v/cm., or

$$\frac{E_1}{E} = 0.20$$

This is the minimum case to have a streamer occur and to cause breakdown.

The breakdown criterion in a uniform field is

$$\alpha\delta + \ln \frac{\alpha}{p} = 14.46 + \ln \frac{E}{p} + \frac{1}{2} \ln \frac{\delta}{p}$$

For a gas in which the pressure is of the order of magnitude of one atmosphere and breakdown potential is applied, a multiplication process of electrons takes place and is termed an electron avalanche. The mechanics of this avalanche have been described (16, 20) as multiplication processes in uniform fields. If the gap is assumed to be one centimeter long and 31,600 volts are applied, the ratio of applied field to gap pressure is 41.6 volts per mm. Hg. Under these conditions an electron acquires a random drift velocity in the direction of the field which has been measured as 1.5×10^7 to 2.7×10^7 cm. per second. Thus, the total time for an electron to cross the gap will be approximately 10^{-7} seconds. Since positive ions have mobilities from 10^{-2} to 10^{-4} less than those of electrons, it will require some 10^{-5} seconds for a positive ion to cross the same gap under the same ambient condition. For a Townsend type discharge to occur it is necessary for these positive ions to cross the gap and strike the cathode which leads to the necessary secondary processes characteristic of this type of breakdown. However, it has been observed that long before 10^{-5} seconds have elapsed, the discharge has occurred and that the total energy to be dissipated has nearly been expended.

In order to explain the breakdown process, the Streamer Theory was postulated. In terms of streamer theory, as the electron avalanche takes place the positive ions left in their wake set up a series of secondary processes which lead to the formation of a highly conducting medium which provides a path for the discharge current in the requisite time. For the example described above a positive streamer forms near

the anode and propagates to the cathode giving the conducting path. The positive streamer is formed by photoelectrons created near the space charge channel of positive ions left by the primary electrons. (It should be noted that the positive space charge column is not a conducting medium, and therefore the avalanche itself does not constitute a breakdown of the gas.) If the electrons created are near the anode, then they are in a favorable position to be accelerated into the space charge region. The electrons from this second type of avalanche in the applied and space charge fields combined are drawn into the space charge channel and form a conducting plasma which starts at the anode and propagates to the cathode. In this instance another electron avalanche is initiated which leaves positive ions behind. These positive ions then extend the space charge region toward the cathode. Thus, the positive space charge develops toward the cathode as a selfpropagating space charge streamer.

The criteria for the formation of a streamer are first that an electron avalanche must have occurred which leaves a positive space charge near the anode. This space charge has its own radial field and will cause photoelectrons to be accelerated to it, thereby allowing propagating as a positive anode streamer to the cathode. Secondly, a sufficient number of electrons must be provided to supply the streamer. These electrons generally exist in the gas near the space charge due to the density of photoionization. This factor depends on the diffusion in the electron avalanche and upon the absorption coefficient of the molecules and/or atoms for the particular energy photons produced in

the avalanche.

The value of the necessary radial field at the space charge tip has been found by Meek to be equal to the impressed external field. He also found that as a general rule this requirement is too stringent and values of the radial field can be from one-tenth to one times the impressed field, depending upon the pressure times distance product and field/pressure ratio of the arc in question.

It has been hypothesized that the total times involved in the formation of positive anode space charge streamers will be much faster than the 10^{-7} seconds postulated for the initial electron avalanche. Cloud track studies by Raether show that the velocity of the secondary electrons being drawn to the space charge region is of the order of 1.3×10^{8} cm/sec as against the 2×10^{7} cm/sec velocity of the initial electrons. As the streamer forms and propagates toward the cathode, intense ionization is produced near the cathode, and as a result an increase in electrons from the cathode should result due to field effect.

As a general statement the streamer theory is then a time-field dependent effect. It is a time effect since the velocity of propagation of the streamer is dependent upon the degree of ionization, and this then allows the establishment of minimum positive ion densities for a streamer to be effective in the gaseous breakdown. It is a field effect due to the fact that the necessary secondary effects are a result of the non-uniform fields developed by the positive space charge column in the gap.

Quantitatively, the requirements for the formation of a positive streamer are as follows:

1. Adequate density of photoionization must exist in the gas near the space charge to provide a continuous supply of electrons.

2. The positive space charge field produced must be such as to draw these photoelectrons into the positive column in sufficient quantity so as to be able to support propagation of the streamer tip.

The Objectives

The main purpose of the work described in this dissertation is an attempt to develop a new and direct technique for measuring the velocity of ions in electrical prebreakdown.

The work has included derivation the complete relativistic Doppler frequency shift equation. In addition the following special purpose measuring circuits were developed.

1. A microwave switch controlling circuit which is able to vary the switching speed within the mechanical limit of the switch. The purpose of this switch is to connect the main input arm and reflected waves to the spectrum analyzer alternatively.

2. A synchronized high voltage pulser which is driven by the rf modulating signal.

3. A microwave reflectometer which must be sensitive enough to detect the moving of ions in the electrical prebreakdown tube.

Use of the microwave Doppler effect to determine translational velocities is hardly a new field, however, this is believed to be the first time that this effect has been used to determine the velocity of positive ions propagating at onset of an electrical discharge.

In this experiment the Doppler shift is determined by sampling

the rf signal from the input side of the bridge and sampling the shifted signal from the detecting arm of the bridge and comparing these on a spectrum analyzer.

CHAPTER III

THEORY

When an electromagnetic wave is incident on a moving body, the frequency of the scattered wave can be shown to differ from that of the incident wave. This is called the "Doppler Effect".

In order to calculate the microwave interaction with particle, the following assumption is made. Let us consider a receiver is in motion with velocity v and fixed in a Cartesian Coordinate (x',y',z',t') as shown in Figure 6.

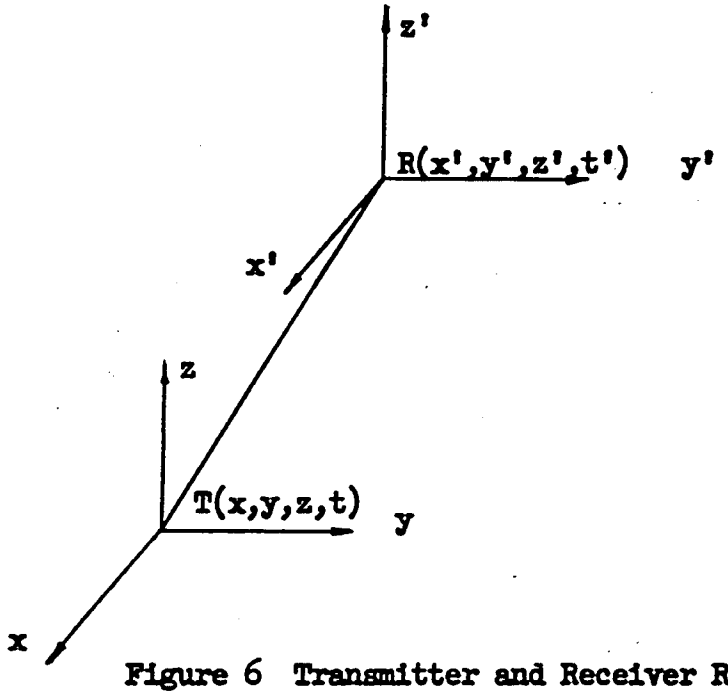

Figure 6 Transmitter and Receiver Relative Position

A transmitter is stationary with Cartesian Coordinate (x,y,z,t) and transmitting an electromagnetic wave $\bar{E} = Ee^{j(\omega t - kz)}$. From Maxwell's equations:

$$\nabla \times \bar{E} = -\mu_o \frac{\partial H}{\partial t} \tag{3-1}$$

$$\nabla \cdot H = 0 \tag{3-2}$$

$$\nabla \times H = \epsilon_o \frac{\partial E}{\partial t} \tag{3-3}$$

$$\nabla \cdot \bar{E} = \frac{\rho}{\epsilon_o} \tag{3-4}$$

$$\bar{I} = \sigma \bar{E} \tag{3-5}$$

$$\nabla^2 \bar{E} = \frac{1}{\mu_o \epsilon_o} \frac{\partial^2 E}{\partial t^2} \tag{3-6}$$

The electromagnetic wave is propagating through the z direction, hence,

$$\nabla^2 \bar{E} = \mu_o \epsilon_o \frac{\partial^2 \bar{E}}{\partial t^2}$$

$$= \frac{1}{\frac{1}{\mu_o \epsilon_o}} \frac{\partial^2 \bar{E}}{\partial t^2}$$

$$= \frac{1}{c^2} \frac{\partial^2 \bar{E}}{\partial t^2} \tag{3-7}$$

From Figure 6

$$z' - z = vt'$$

$$r^2 = \overline{TR}^2 \tag{3-8}$$

$$\overline{TR}^2 = (x' - x)^2 + (y' - y)^2 + (z' - z)^2$$

$$= c^2 (t - t')^2 \tag{3-9}$$

Differentiating (3-9) gives

$$2(z - z')(dz - dz') = 2c^2(t - t')(dt - dt') \tag{3-10}$$

Since

$$c(t - t') = r \tag{3-11}$$

$$(z - z') = vt' \tag{3-12}$$

Simplifying (3-10), yields

$$(z - z')(dz - dz') = c^2(t - t')(dt - dt') \tag{3-13}$$

Substituting equations (3-11) and (3-12) into (3-13), gives

$$(z - z')vdt' = cr(dt - dt')$$

$$\left(1 + \frac{z - z'}{r} \frac{v}{c}\right) dt' = dt \tag{3-14}$$

Let dt" be the time interval corresponding to dt' for an observer at rest with respect to R, then taking the Lorentz Transformation (33, 4, 3)

$$t_1' = \beta \left(t_1'' + \frac{vx_1''}{c^2}\right) \tag{3-15}$$

$$t_2' = \beta \left(t_2'' + \frac{vx_1''}{c^2}\right) \tag{3-16}$$

where $\beta = \dfrac{1}{\sqrt{1 - \dfrac{v^2}{c^2}}}$

Substracting equation (3-16) from (3-15), gives

$$t_2' - t_1' = \beta \left(t_2'' - t_1''\right)$$

or simply

$$dt' = \beta dt'' \tag{3-17}$$

Dividing (3-14) by (3-17), result is

$$\frac{dt}{dt''} = \beta\left(1 + \frac{z - z'}{r} \frac{v}{c}\right) \tag{3-18}$$

Also from Lorentz Transformation,

$$t = \beta\left(t' + \frac{vx'}{c^2}\right)$$

for $v \ll c$, $t = t'$ and

$$\frac{dt}{dt''} = \beta\left(1 + \frac{z - z'}{r}\frac{v}{c}\right)$$

or

$$\frac{f''}{f} = \beta\left(1 + \frac{\bar{u}\cdot\bar{v}}{c}\right) \qquad (3\text{-}19)$$

where $\bar{u}$ is the unit vector in the direction of propagation. Thus it is found that the novel feature as compared with the classical results is the appearance of the factor β. From (3-19)

$$\frac{f''}{f} = \frac{1 + \frac{\bar{u}\cdot\bar{v}}{c}}{\sqrt{1 - \frac{v^2}{c^2}}}$$

$$= \left(1 + \frac{\bar{u}\cdot\bar{v}}{c}\right)\left(1 - \frac{v^2}{c^2}\right)^{-1/2}$$

$$= \left(1 + \frac{\bar{u}\cdot\bar{v}}{c}\right)\left(1 + \frac{1}{2}\frac{v^2}{c^2} \ldots\ldots\right) \qquad (3\text{-}20)$$

If a microwave beam is reflected from a moving mirror, we may think of the image as a source which is moving with twice the velocity of the mirror. If $\bar{u}\cdot\bar{v}$ is the component of the velocity of the moving observer toward the source, then, (3-20) can be written as:

$$\frac{f''}{f} = \left(1 + 2\,\frac{\bar{u}\cdot\bar{v}}{c}\right)\left(1 + \frac{1}{2}\,\frac{v^2}{c^2} \ldots\ldots\right) \qquad (3\text{-}21)$$

where f'' and f are the shifted and unshifted frequencies which will be

explained in more detail in the following paragraphs.

When a modulating signal is combined with the carrier, the amplitude modulated carrier can be represented as

$$f_c(t) = K(1 + m\cos \omega_m t)(\cos \omega_c t)$$

where

ω_c is the carrier frequency

ω_m is the modulating signal frequency

$$\omega_c \gg \omega_m$$

m is modulating index

then

$$f_c(t) = K \cos \omega_c t + \frac{K}{2} m \cos(\omega_c + \omega_m) + \frac{K}{2} m \cos(\omega_c - \omega_m)t \qquad (3\text{-}22)$$

where $(\omega_c + \omega_m)$ is the upper sideband

$(\omega_c - \omega_m)$ is the lower sideband

The carrier frequency, the upper sideband and lower sideband (32) can be plotted as Figure 7.

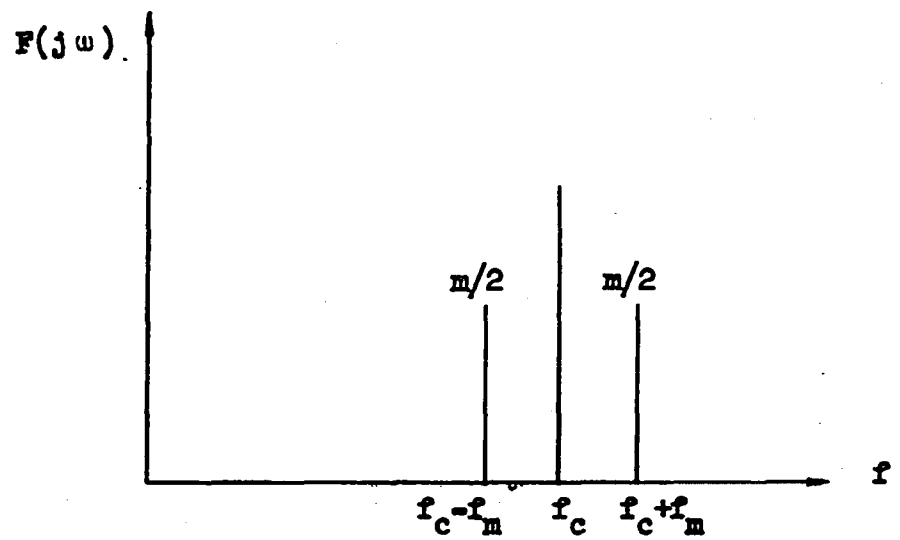

Figure 7 AM Frequency Spectrum

For periodic input, f(t), the alternative form of the Fourier series expansion may be written as

$$f(t) = \frac{1}{T} \sum_{n=-\infty}^{\infty} c_n e^{j \omega_n t} \qquad (3\text{-}23)$$

Let us consider the series of pulses as shown in Figure 8

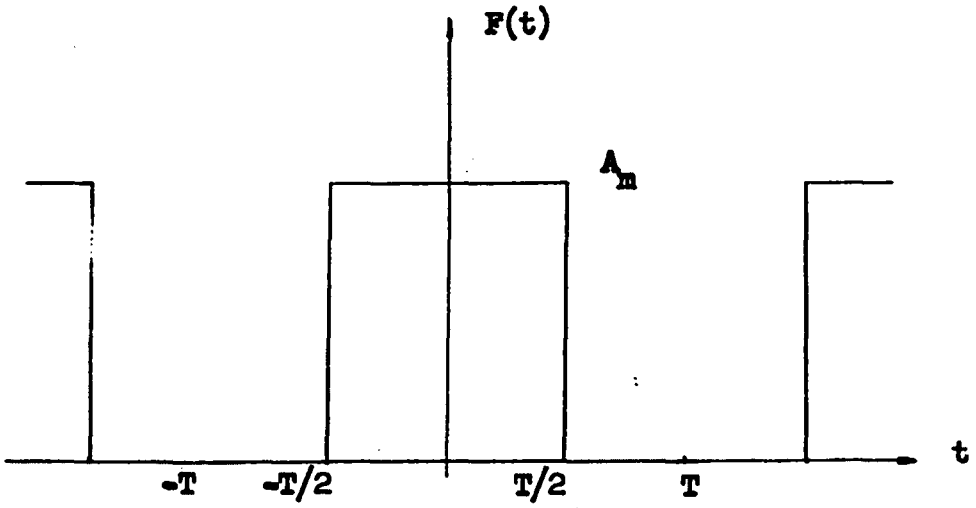

Figure 8 Fourier Analysis of Rectangular Wave

where $$c_n = \int_{-\frac{T}{2}}^{\frac{T}{2}} A_m e^{-j \omega_n t} dt$$

$$= \frac{2A_m}{n} \sin \frac{\omega_n T}{2}$$

$$= TA_m \frac{\sin\left(\frac{\omega_n T}{2}\right)}{\frac{\omega_n T}{2}}$$

Let $$x = \frac{\omega_n T}{2}$$

$$c_n = TA_m \frac{\sin x}{x}$$

A plot of $(\frac{\sin x}{x})$ versus x is shown in Figure 9

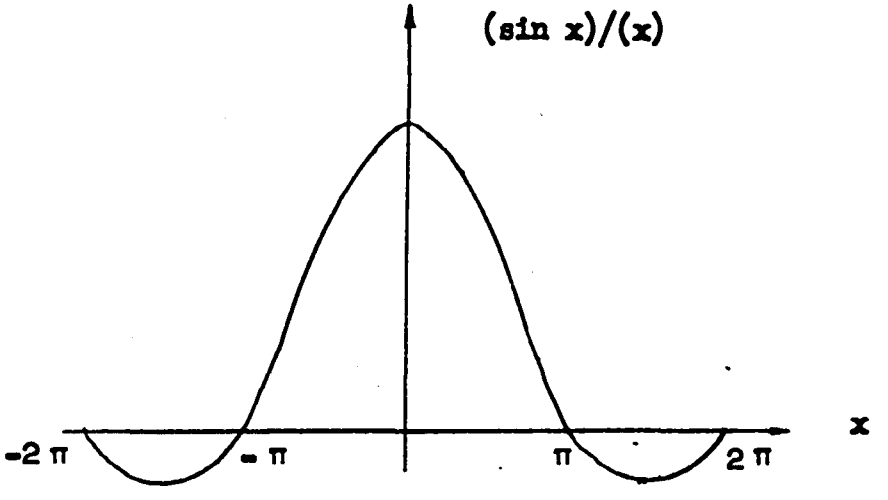

Figure 9 (sin x)/x Versus x

therefore a perfect rectangular pulse of rf energy would display the spectrum as shown in Figure 9. In practice, the spectrum departs from the $\frac{\sin x}{x}$ function due to finite rise and decay characteristics of the pulse. Actually, the spectrum analyzer does not display phase information and therefore the lobes below the axis appear inverted above the axis on the display as shown in Figure 10.

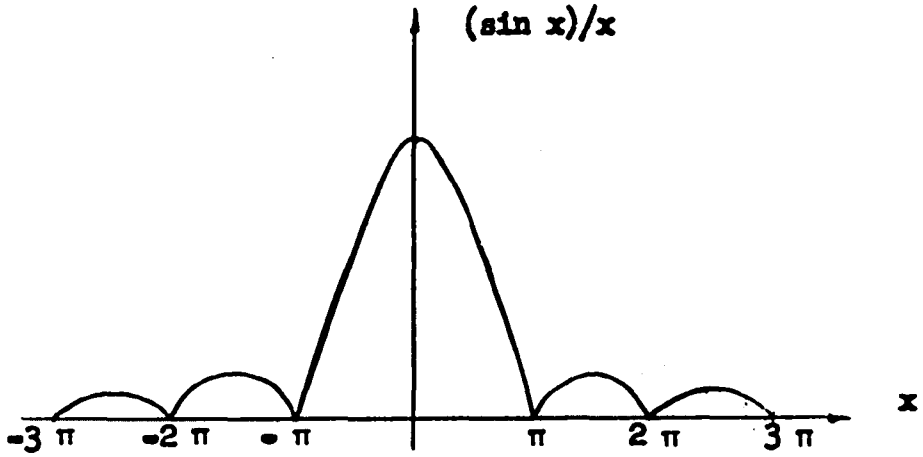

Figure 10 (sin x)/x Versus x Shown in Spectrum Analyzer

For a generalized periodic input

$$f(t) = \frac{1}{T} \sum_{n=-m}^{m} |c_n| \, e^{j \omega_n t}$$

$$= \frac{2}{T} \sum_{n=1}^{m} |c_n| \cos (\omega_n t + \theta_n) \qquad (3\text{-}25)$$

With zero average value (i.e. no dc component), then

$$f_c(t) = K \left[1 + \frac{2m}{T} \sum_{n=1}^{m} |c_n| \cos(\omega_n t + \theta_n) \right] \cos \omega_c t \qquad (3\text{-}26)$$

The AM signal, thus consists of the unmodulated carrier plus the double sideband terms.

$$f_c(t) = K \cos \omega_c t + \frac{mK}{T} \sum_{n=1}^{m} | c_n | \cdot \left[\cos \left[(\omega_c + \omega_n)t + \theta_n \right] + \cos \left[(\omega_c - \omega_n)t - \theta_n \right] \right] \qquad (3\text{-}27)$$

The amplitude-modulated frequency spectrum appears in Figure 11.

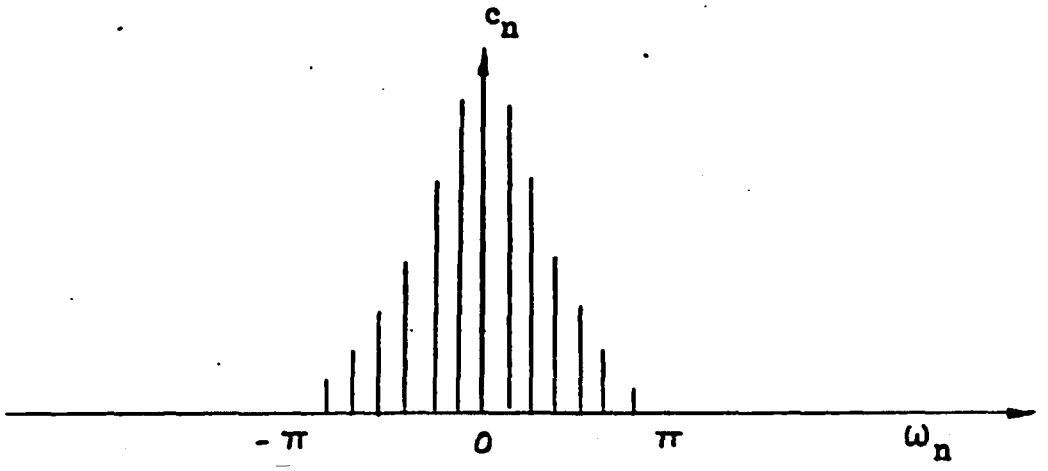

Figure 11 Amplitude-Modulated Frequency Spectrum

If the frequency shift is detectable, after applying the high voltage to the ionization tube, the comparison of the shifted spectrum with the unshifted spectrum will be as shown in Figure 12.

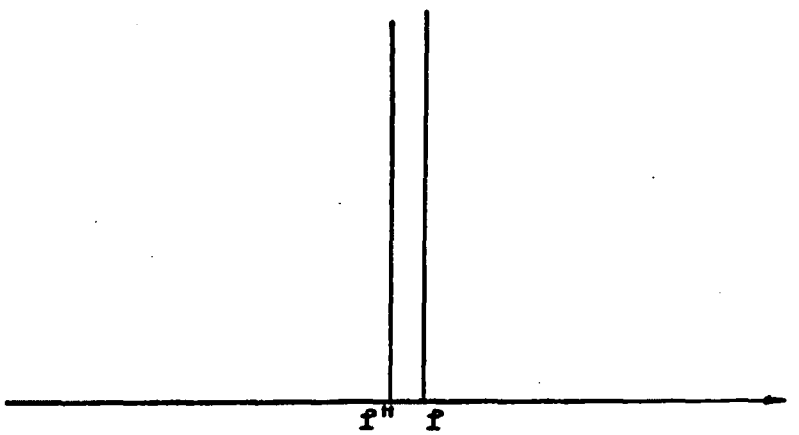

Figure 12 The Comparison of The Spectrum

From Figure 12, f" - f is the Doppler frequency shift Δf. According to equation (3-21), Δf can be written as follow:

$$\Delta f=(2fv/c)\ (\ 1+(1/2)v^2/c^2+(1/2)v^3/c^3+.....) \qquad (3\text{-}28)$$

where Δf is the Doppler frequency shift

f is the carrier frequency

v is the velocity of the ion

If Δf can be found, then the velocity of the positive ions can be calculated by means of equation (3-28).

The cross-section of targets of ions

Let us assume the air inside the ionization tube is ionized uniformly and simultaneously. The ionized nitrogen (3/4 of the air is nitrogen) molecules form a grid screen as shown in the following

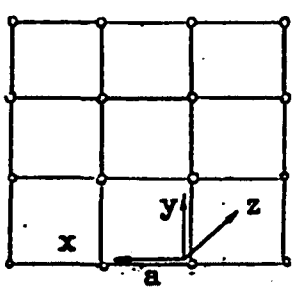

The screen will reflect the incident wave. The cut off frequency of the propagating TE_{10} wave is a function of the dimension of the grid a, as shown in equation (3-29)

$$2\pi f_c \sqrt{\mu_o \epsilon_o} = \frac{n}{a} \qquad (3\text{-}29)$$

where f_c is the cut off frequency and equal to 33.5 kmc.

n is chosen to be the minimum integer 1.

$$\frac{2f_c}{c} = \frac{1}{a}$$

$$\frac{2 \times 33.5 \times 10^9}{3 \times 10^{10}} = \frac{1}{a}$$

$$a = \frac{30}{67} = 0.448 \text{ cm}$$

Since the nitrogen molecules are ionized uniformly and simultaneously, it is reasonable to assume the screen is formed as a square. For a unit area 1 cm^2, there are

$$\frac{1}{0.448} = 2.2 \doteq 2 \text{ molecules/ cm}$$

on each side, therefore, the total number of molecules per unit area are

$$4 \times 2 = 8 \text{ molecules/cm}^2$$

the minimum dinsity of the ionized nitrogen molecules for detection by a 33.5 kmc signal is equal to 8 molecules/cm^2.

The resolution of the spectrum analyzer

By definition, the resolution is the 3 db IF bandwidth, however, it does take into consideration other factors. It can be shown that, for an assumed Gaussian IF response, the effective resolution, R is equal to

$$R = B \left[1 + 0.195 \left(\frac{F}{TB} \right)^2 \right]^{1/2} \qquad (3\text{-}30)$$

where B = 3 db IF bandwidth in cps.

F = the dispersion in cps.

T = sweep - time interval in second.

Under normal operation,

B = 1 — 80 kc.

F = 25 kc — 10 mc.

T = $1-\frac{1}{30}$ sec.

$$R = 80{,}000 \left[1 + 0.195 \left[\frac{10 \times 10^6}{\frac{1}{30} \times (80 \times 10^3)^2} \right]^2 \right]^{1/2}$$

$$= 80{,}000 \left[1 + 0.195 \left(\frac{30}{64} \right)^2 \right]^{1/2}$$

$$\doteq 80{,}000 \text{ cps.}$$

CHAPTER IV

EXPERIMENTAL TECHNIQUE

The new special experimental technique developed in this research using the Doppler frequency shift is described below:

General Description

The whole experimental apparatus is shown in Figure 13. The block diagram of the experiment set up is shown in Figure 14. The FXR klystron power supply not only delivers the power to the Doppler reflectometer (19, 27), but also gives a synchronizing signal for the trigger of the high voltage pulser, which are locked together. The microwave switch is operating at its maximum mechanical speed limit of about 10 cps. The lowest pressure that the vacuum pump can attain in the discharge tube is 0.15 mm Hg. Air is used as a medium. The maximum operating frequency of the spectrum analyzer is 68 kmc, however the frequency response is limited by the klystron operating range of 32 to 38 kmc.

The detailed circuit analysis is explained in the following sections.

Figure 13 Photograph of the Experimental Appartus

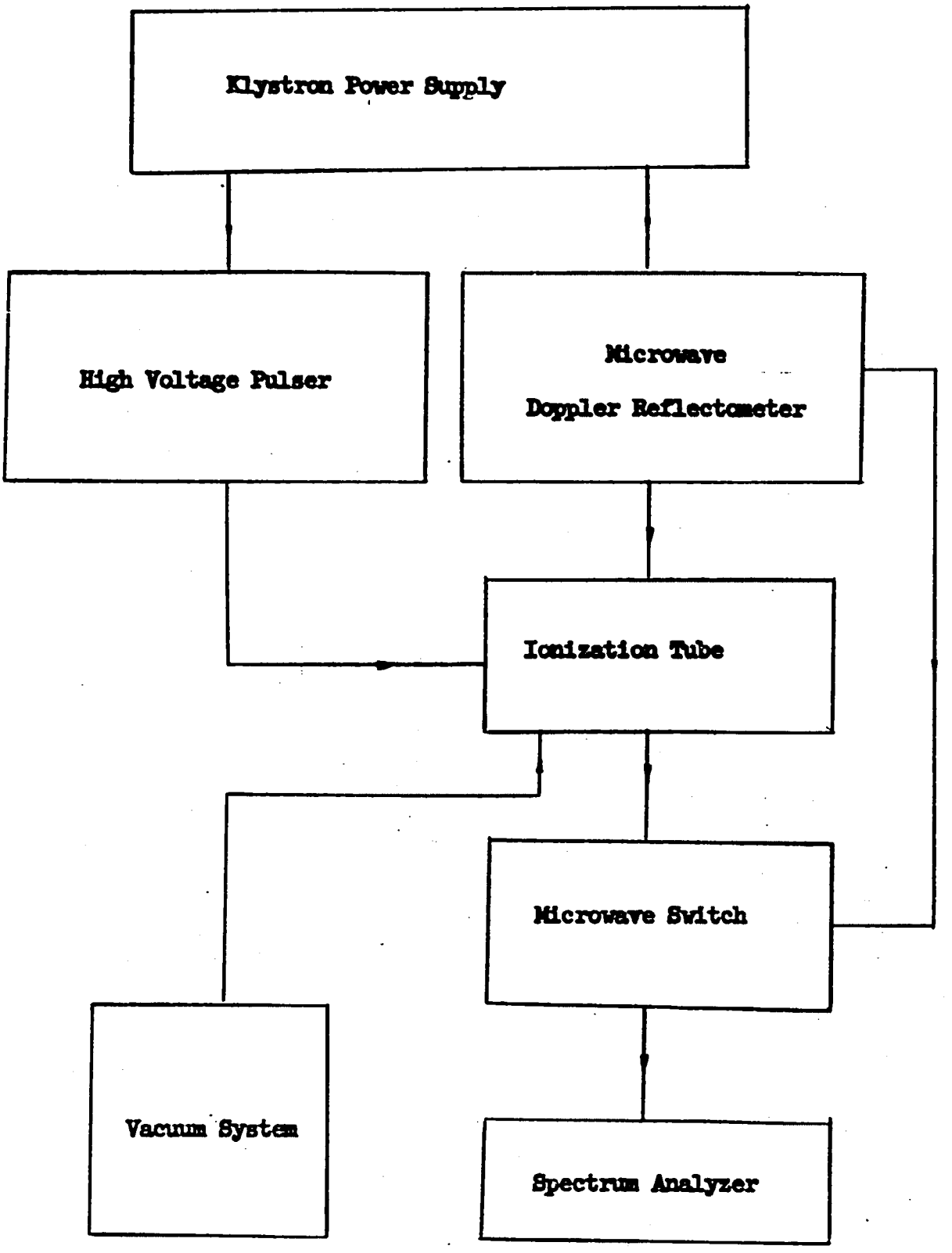

Figure 14 The Block Diagram of Experimental Set Up

Detailed Description of the Apparatus

The main parts described in the following sections will include:

1. Microwave switch controlling circuit.
2. High voltage synchronized pulser.
3. Doppler reflectometer.
4. Vacuum system and ionization tube.
5. Spectrum analyzer.

1. Microwave switch controlling circuit

The purpose of this design is to control the speed of the switch which connects the main input signal and the reflected signal to the spectrum analyzer alternatively. The frequency of switching is controlled by an unijunction transistor pulser, while the switching power input is controlled by a pair of silicon control rectifiers. The block diagram is shown in Figure 15.

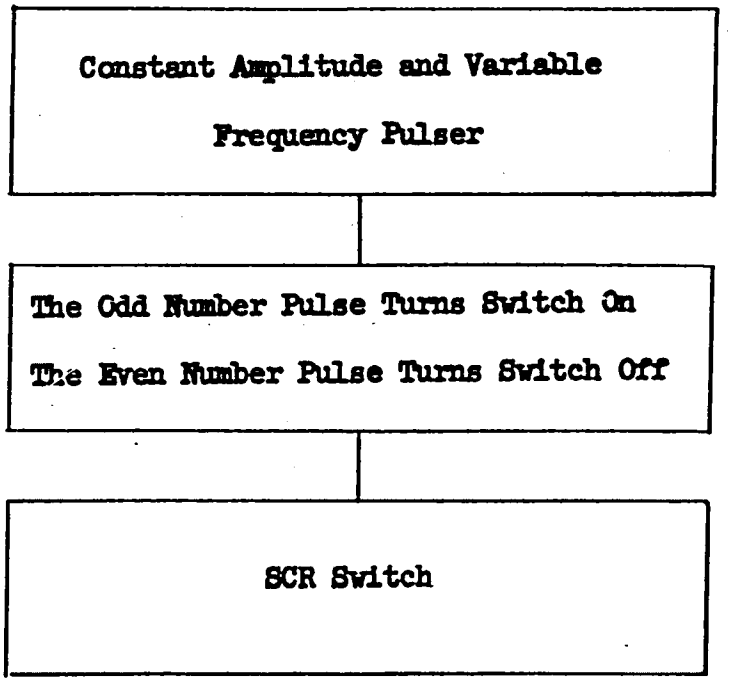

Figure 15 Microwave Switch Control

The pulser will give a rough frequency range. A unijunction transistor is used to generate the bootstrap sweep. By varying its time constant, a constant amplitude variable frequency pulse is available.

A. Variable frequency pulser

(i) Bootstrap circuit (10): A typical bootstrap circuit which will generate a constant amplitude and frequency linear sawtooth waveform as shown in Figure 16.

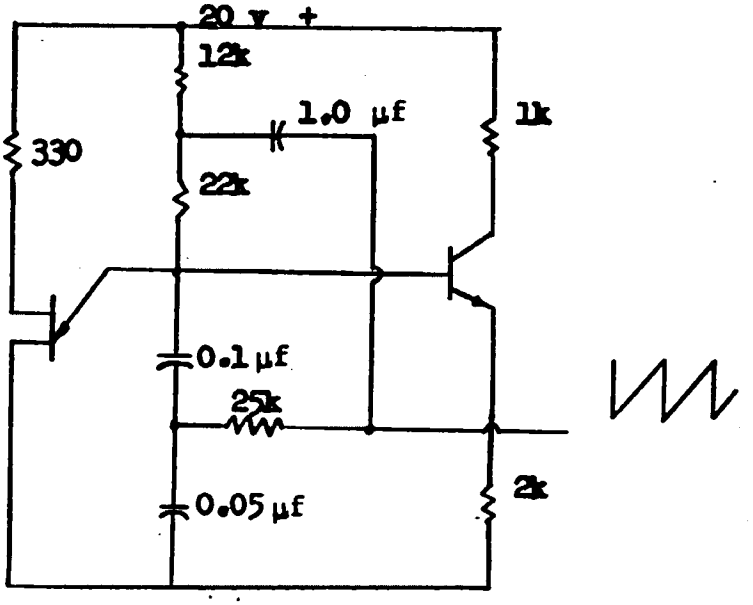

Figure 16 Bootstrap Circuit

(ii) Frequency control circuit: In the circuit shown in Figure 17, an additional transistor Q_2 is employed to vary the charging rate of the capacitor, and a frequency ratio of 10:1 obtained. The original circuit is shown in Figure 17.

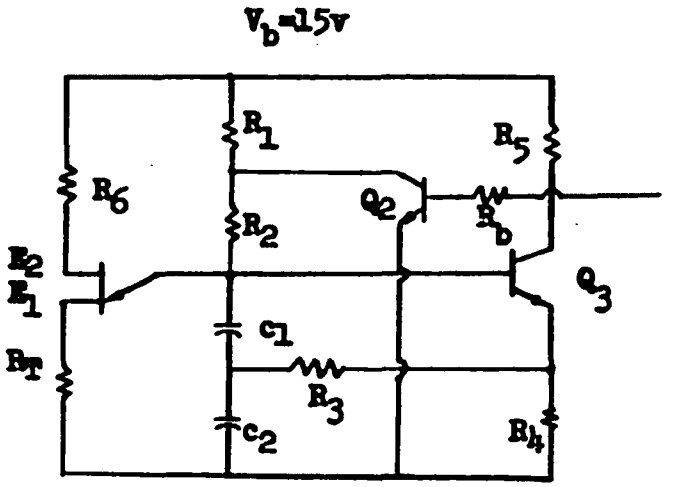

Figure 17 The Modified Bootstrap Sweep Circuit

The equivalent circuit is shown in Figure 18

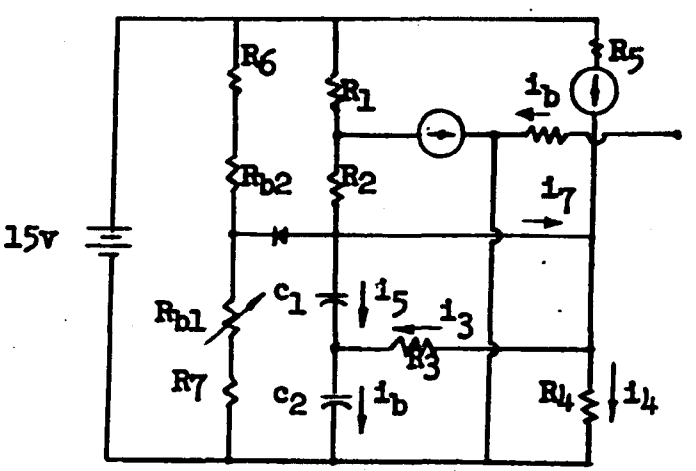

Figure 18 The Equivalent Circuit of Figure 17

The whole circuit can be represented by the following equation:

$$0.97\,E_1(s) - E_2(s) = R_3 I_3(s) \tag{4-1}$$

$$I_1(s) = I_2(s) + \beta\, I_b(s) \tag{4-2}$$

$$E_1(s) = \frac{1}{c_1 s}\, I_5(s) + E_2(s) \tag{4-3}$$

$$E_2(s) = \frac{1}{c_2 s}\, I_5(s) + I_3(s) \tag{4-4}$$

$$R_2 I_2 = V_b(s) - R_1 I_1(s) - E_1(s) \tag{4-5}$$

$$I_3(s) + \frac{0.97}{R_4}\, E_1(s) = \beta_2 I_5(s) - \beta_2 I_2(s) \tag{4-6}$$

Algebric manipulation, gives

$$E_1(s) = \frac{W \cdot c(c_1 + c_2)\left(s + \dfrac{1}{R_3(c_1 + c_2)} \right)}{s\left[s^2 + s \cdot X - Y - Z \right]} \tag{4-7}$$

where

$$W = \frac{V_b - \beta\, R_1 I_b(s)}{c_1 c_2 (R_1 + R_2)}$$

$$X = \frac{0.03 c_1 (1 + \beta) - 0.97 c_2}{c_1 c_2 \beta_2 R_3}$$

$$Y = \frac{(c_1 + c_2)\left[\dfrac{0.97}{R_4}\,(R_1 + R_2) - \beta \right]}{c_1 c_2 \beta_2 (R_1 + R_2)}$$

$$Z = \frac{\dfrac{0.97}{R_4}\,(R_1 + R_2) - \beta}{c_1 c_2 \beta_2 R_3 (R_1 + R_3)}$$

From Figure 19, by setting

$R_1 + R_2 = 40\ K$ $\qquad$ $E_1 = 15\ v$

$c_1 = c_2 = 1\ \mu f$ $\qquad$ $R_3 = K\Omega$

and from equation (4-7)

$$E_1(S) = \frac{50(15 + 26I_bR_1)(S + \frac{500}{R_3})}{S\left[S^2 + S(33.5 - \frac{7.6}{R_3}) + \frac{1.675}{R_3} x10^4\right]}$$

By setting $R_3 = 12\ K$

$$E_1(S) = \frac{50(15 + 26I_bR_1)(S + 41.6)}{S\left[S^2 + S(33.5 - 0.634) + 0.14 \times 10^4\right]}$$

$$e_1(t) = 1.5(15 + 26I_bR_1)\left[1 - e^{-16.5t}(\cos 33.6t - 0.5\sin 33.6t)\right] \quad (4\text{-}8)$$

A plot of $e_1(t)$ versus time in millisecond is shown in Figure 20. The waveform of $e_1(t)$ versus time is shown in Figure 21.

(iii) Change of frequency range: In order to change the frequency, it is necessary to vary the size of the two capacitors to

$$\text{new capacitor} = 1\ \mu f \times \frac{\text{original lower end frequency(200 cps)}}{\text{new lower end frequency}}$$

In order to work on the linear portion of the response function $e_1(t)$, it is necessary to reverse the βI_b direction. The output frequency ratio of E_{b1} will then be directly proportional to the current input. This can be accomplished by utilizing the circuit shown in Figure 19.

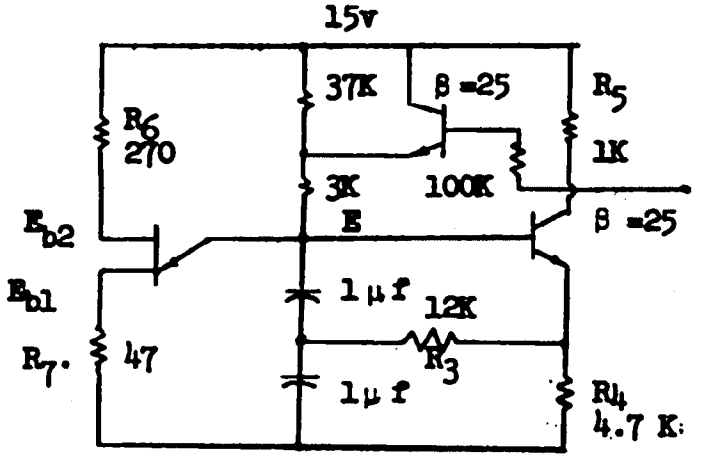

Figure 19 Final Circuit

Time \ Value	A	B	C	D	E	F	G	H
.001	.0165	.983	1.9	.99939	.0349	.0175	.000	.000
.003	.0495	.951	5.7	.99494	.1004	.0502	.902	.097
.009	.1485	.862	17.3	.95476	.2973	.1486	.694	.306
.012	.1980	.820	23.1	.91982	.3934	.1861	.602	.398
.015	.2475	.781	28.9	.87456	.4832	.2416	.495	.505
.018	.2970	.743	34.7	.82214	.5692	.2846	.398	.602
.019	.3135	.731	36.0	.80282	.5962	.2981	.368	.632
.020	.3300	.718	38.5	.78261	.6225	.3112	.338	.662

Table 1 Calculated Value of Equation (4-8)

$A = 16.5t$ $B = e^{-16.5t}$ $C = 33.6t$

$D = \cos 33.6t$ $E = \sin 33.6t$ $F = 0.5 \sin 33.6t$

$G = e^{-16.5t}(\cos 33.6t - 0.5 \sin 33.6t)$

$H = e_1(t)/K$

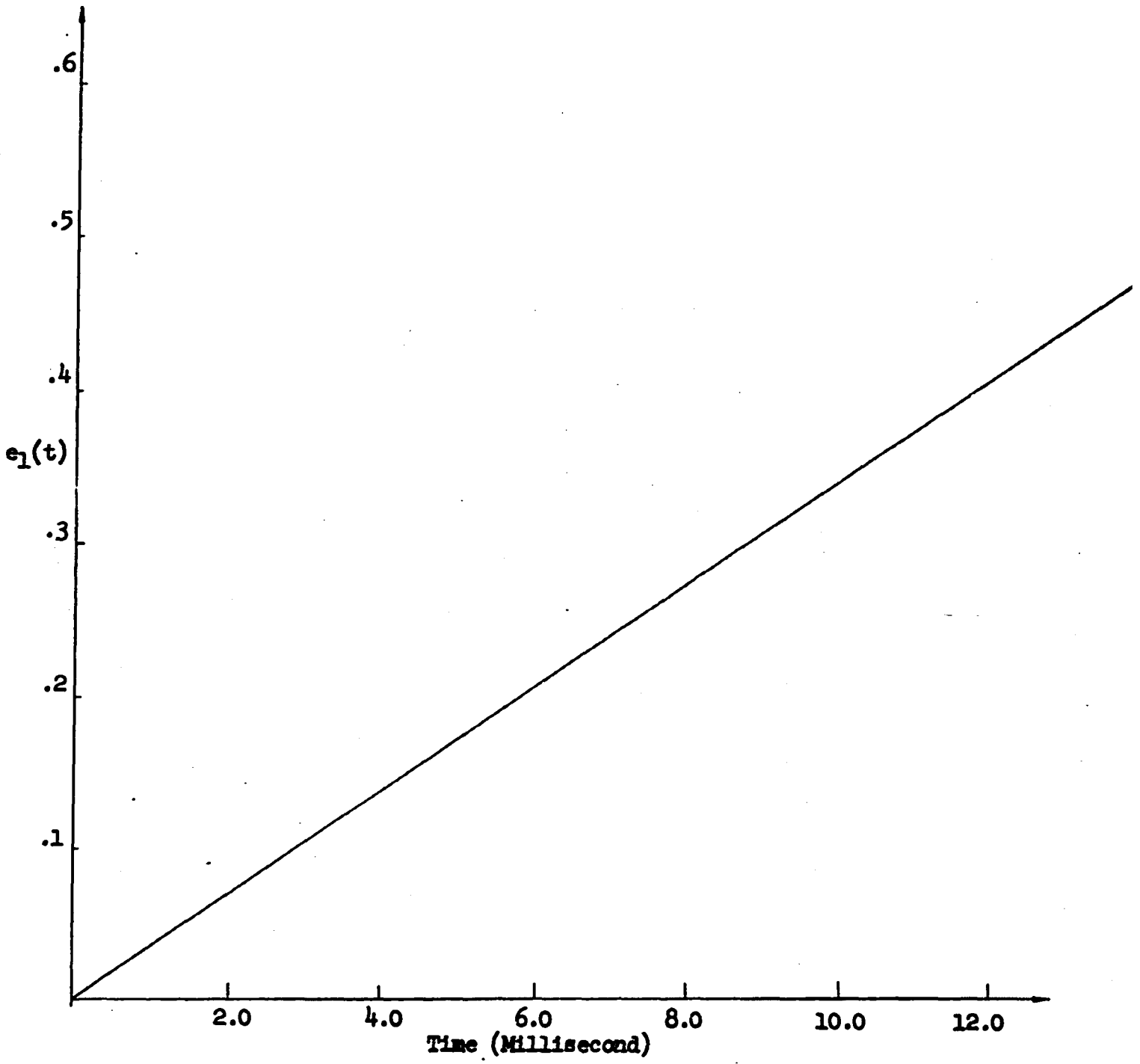

Figure 20 $e_1(t)$ Versus Time

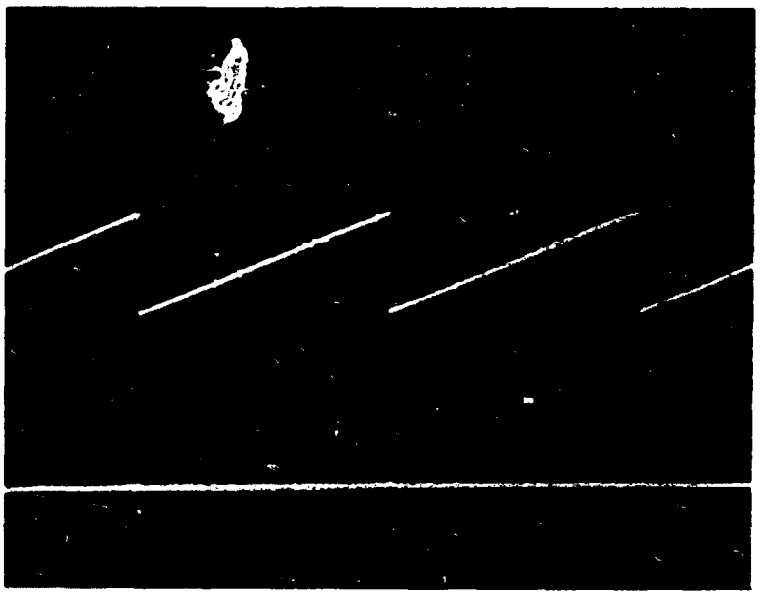

Figure 21 Constant Amplitude Varying Frequency Pulser
Upper trace, Sawtooth Waveform
Lower trace, Pulse Waveform

B. SCR Control Circuit (11,18)

The pulser will give a train of pulses only. In order to select the odd number pulses for turning on the SCR and the even number pulses for turning off the SCR, a binary flip-flop (15) as shown in Figure 22 is used. When transistor T_1 is turned on, T_2 is turned off. The leading edge of the square wave is used for turning on the SCR while the trailing edge of the square wave is used for turning off the SCR.

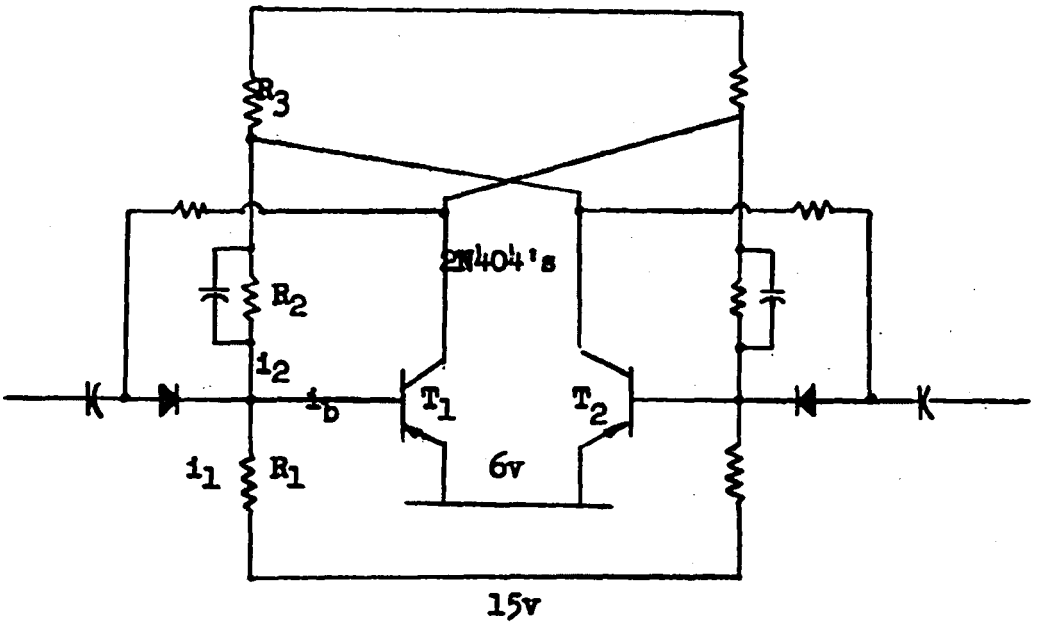

Figure 22 Flip-flop

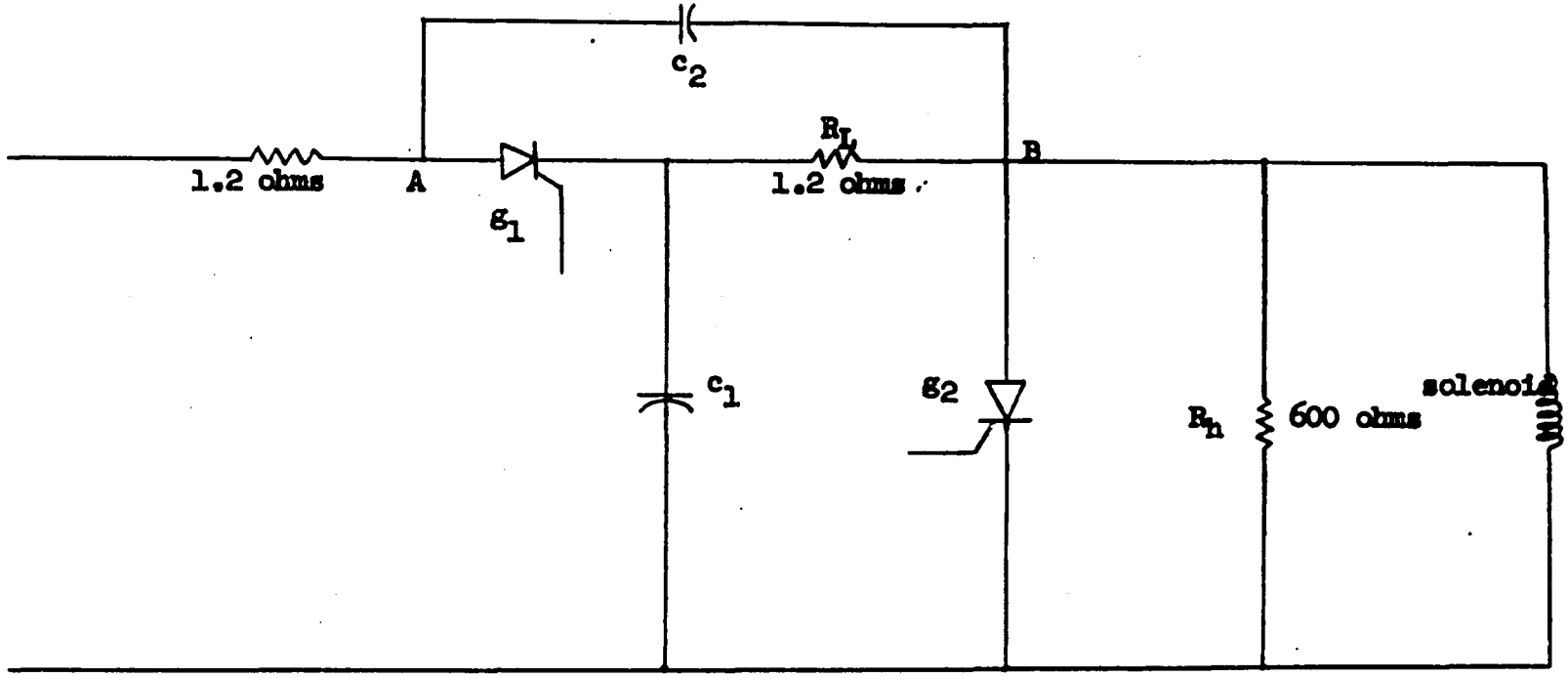

Figure 23 SCR Switching Circuit

Assume T_1 is saturated

$$R_1 = \frac{E_{cc} - E_{bb}}{0.5}$$

$$= \frac{15 - 5}{0.5}$$

$$= 20 \text{ K}$$

$$i_1 = \frac{5}{20 \text{ K}}$$

$$= 0.5 \text{ ma}$$

$$i_2 = i_1 + i_b$$

$$= 0.5 + 0.4 = 0.9 \text{ ma}$$

$$R_2 + R_3 = \frac{5}{0.9} = 5.5 \text{ K}$$

Choose 5.1 K

$$V_{\text{base } 2} = 5 + 10 \frac{5.1}{25.1} = 7.5 \text{ v}$$

therefore, T_2 is off.

C. SCR switching circuit

The detailed circuit is shown in Figure 23. When g_1 is pulsed, SCR_1 is conducting and the solenoid is energized, the switch is turned on and when g_2 is pulsed SCR_2 is conducting. Point B and A of Figure 23 is ground at this instant but c_1 still maintains the B+ voltage, therefore the SCR_1 is cut off. The waveform of the switch is shown in Figure 24.

Generally speaking, an SCR can be turned on by pulses. In order to operate properly with inductive loads, the gating signals applied to the silicon control rectifiers must be square waves rather than pulses, therefore the collector T_1 of Figure 22 is directly connected to g_1 through a diode.

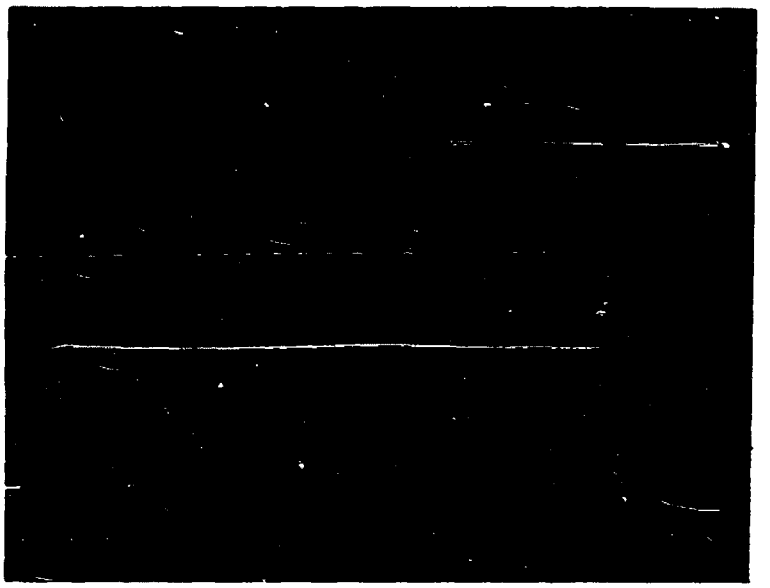

Figure 24 The SCR Switch Waveform
Upper trace, Input rf Signal (0.1v/cm)
Lower trace, SCR Switch Waveform (10 v/cm)

The collector T_2 of Figure 22 is differentiated and then connected to g_2 through another diode.

During the turn-on period, the protection of SCR by means of fuses can be inadequate. The fuse ratings are based on the I^2t rating of SCR, which is derived from the data taken with the whole junction turned on. Therefore the fuses do not necessarily protect the SCR from the effects of localized heating.

The resistance R_h used in Figure 23, is an attempt to improve the wave form. The current drawn by the switch is about 0.2 amp. and will vary with the applied terminal voltage.

2. Synchronized high voltage pulser

In order to synchronize the high voltage pulser with the rf input, the pulser must be driven by the modulated rf signal. A block diagram is shown in Figure 25 and 27. To avoid a loading effect, an isolating stage is required. In order to have a wide operating range of the modulating signal, an amplifier is followed after the isolating stage. The simplest phase shift control can be obtained by an RC circuit, where R is a variable, and depends on the degree of the phase shift. The detailed circuit diagram is shown in Figure 26 and 28. Control of the SCR circuit is slightly different from that discussed in Section 1. Since a pulse output is required, the connection of the transformer is directly across the resistance R_L as shown in Figure 28. During the turn on and turn off period, the pulser will always give a positive pulse. The test data are listed in Table 2.

Table 2 The Test Data of High Voltage Pulser

V_{dc}(v)	I_{dc}(ma)	Pulse Voltage(Kv)
5	63	0.81
10	130	1.65
15	220	2.90
20	315	4.60
25	400	6.20
30	505	9.10
35	620	12.00
40	740	14.00

The overall waveform is shown in Figure 29 and 30.

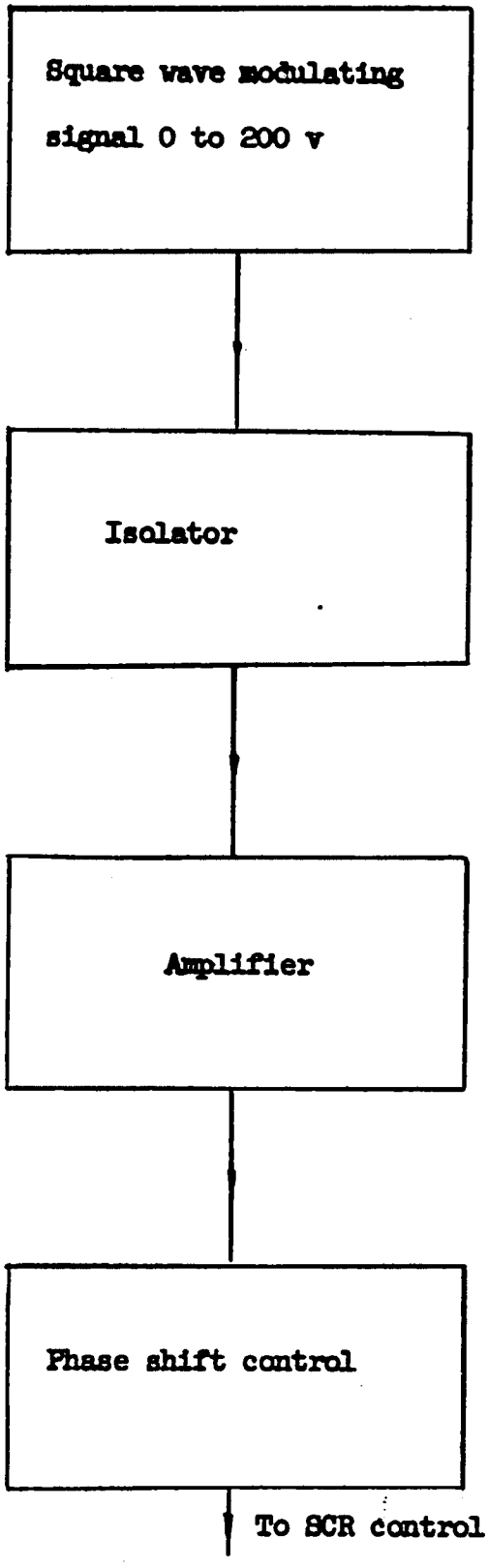

Figure 25 Square Wave Phase Shifting Control

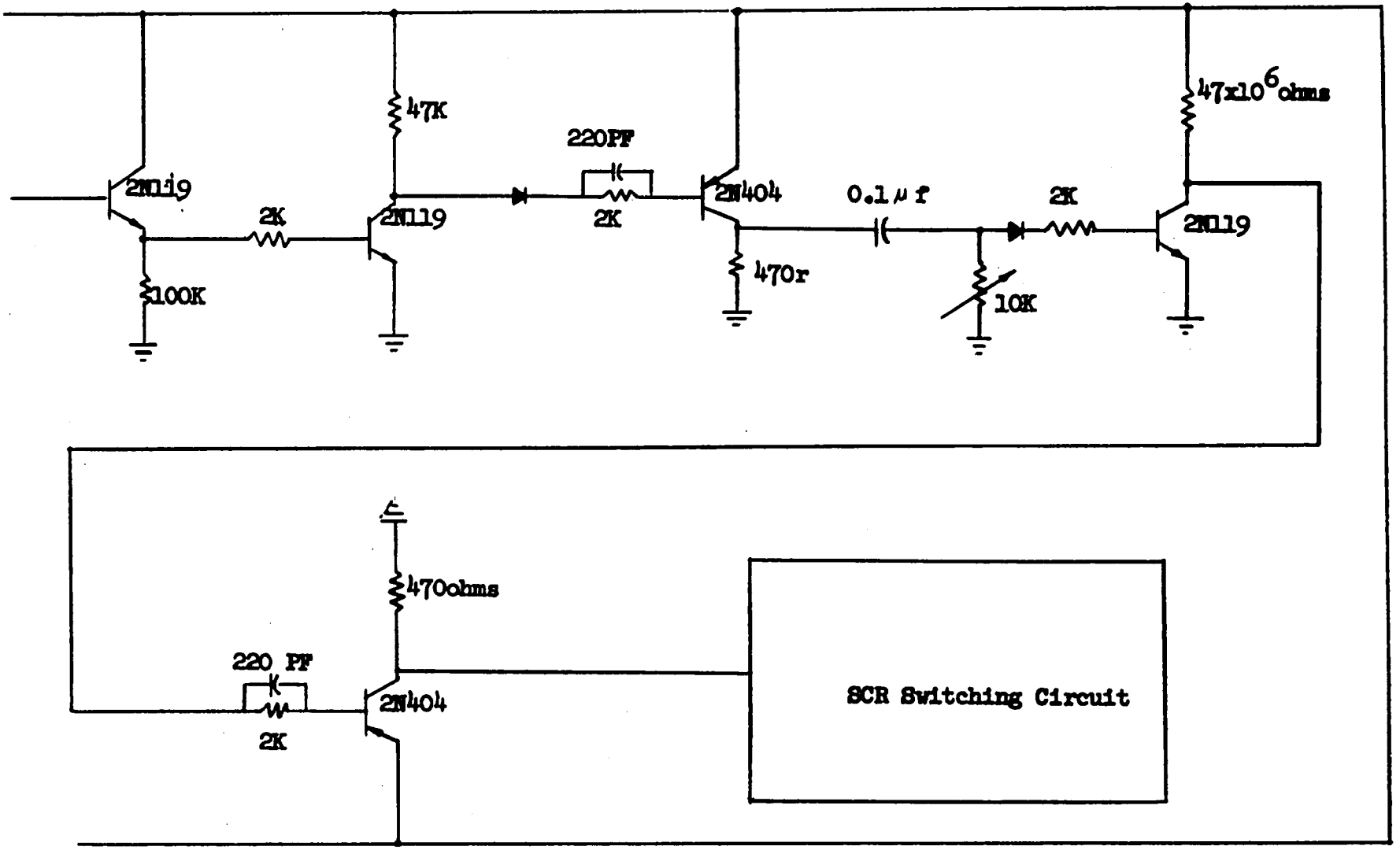

Figure 26 Detailed Circuit For Square Wave Phase Shifting Control

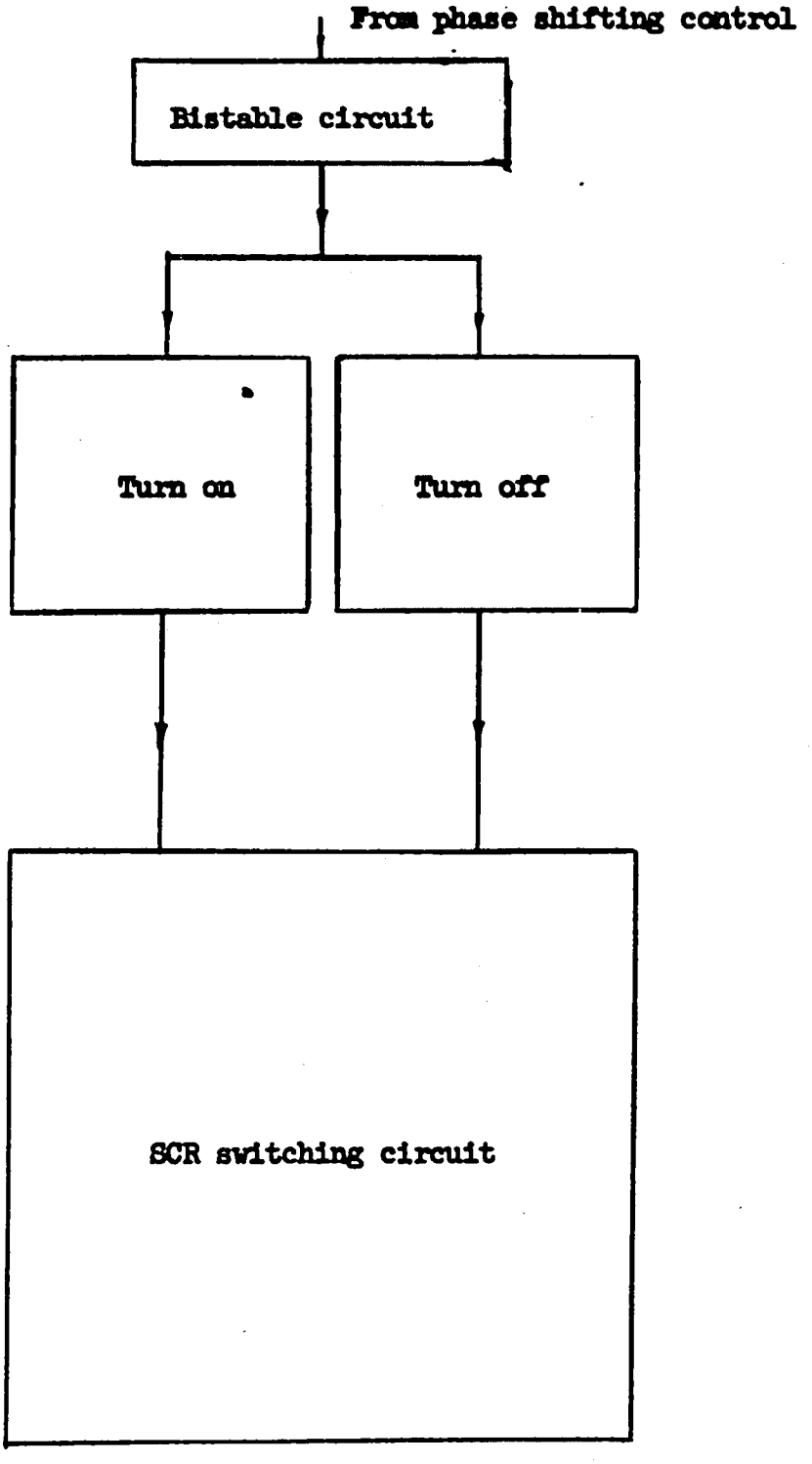

Figure 27 SCR Control Circuit

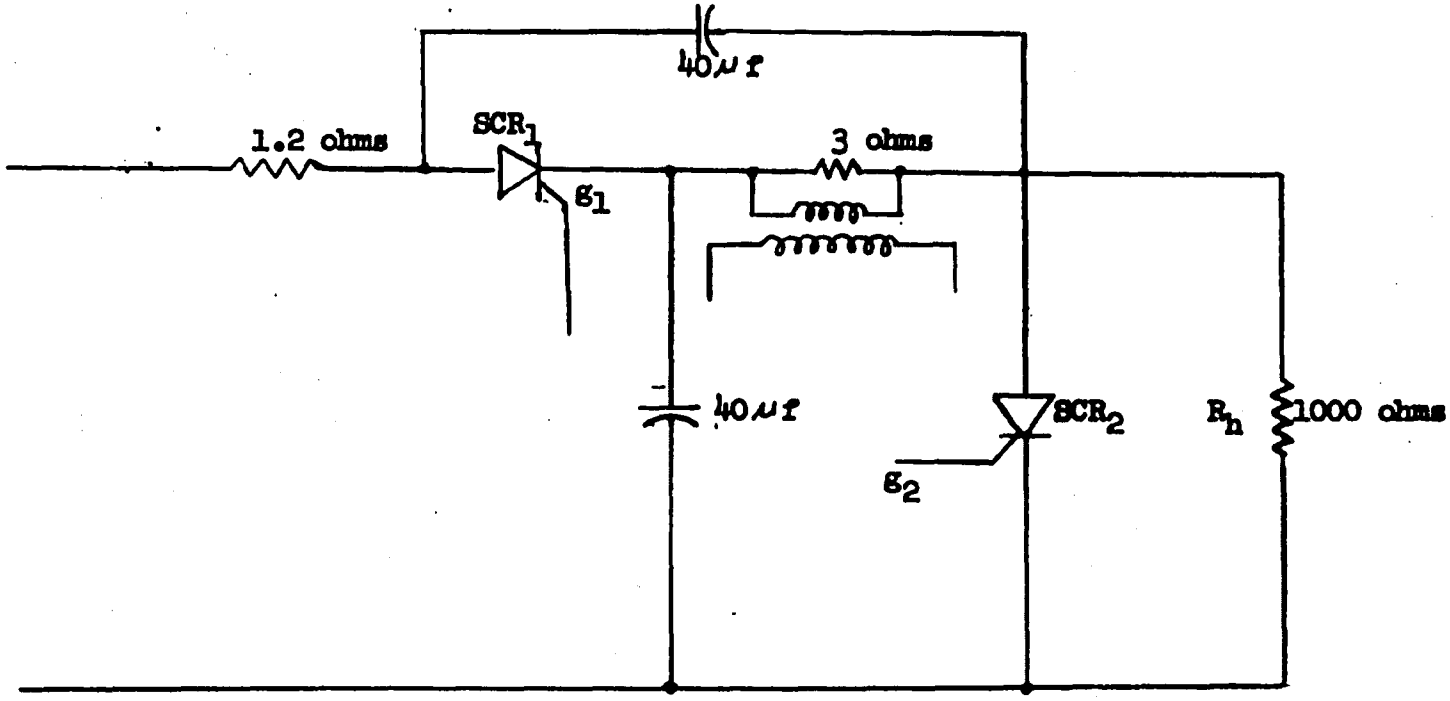

Figure 28 High Voltage Pulser

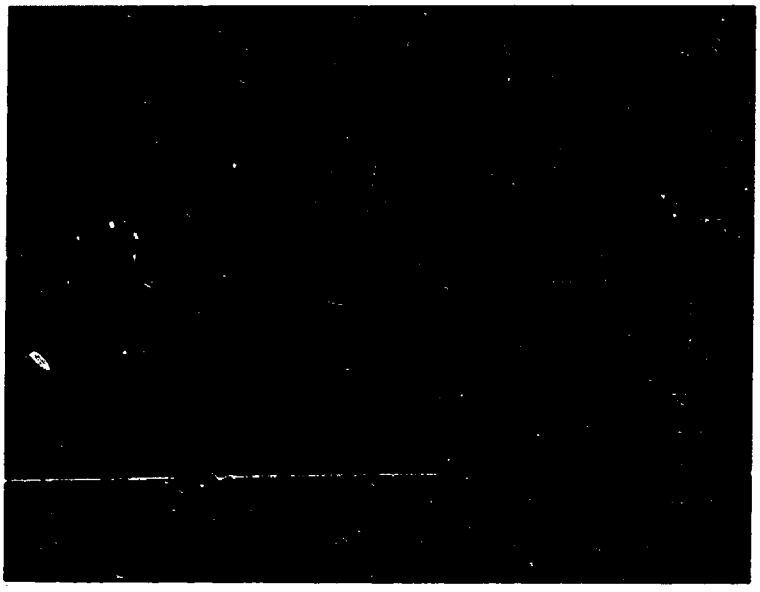

Figure 29 The High Voltage Pulse and The rf Modulating Signal
Upper trace, Modulating Signal (1 v/cm)
Lower trace, High Voltage Pulse (2 kv/cm)
Time, 1 msec/cm

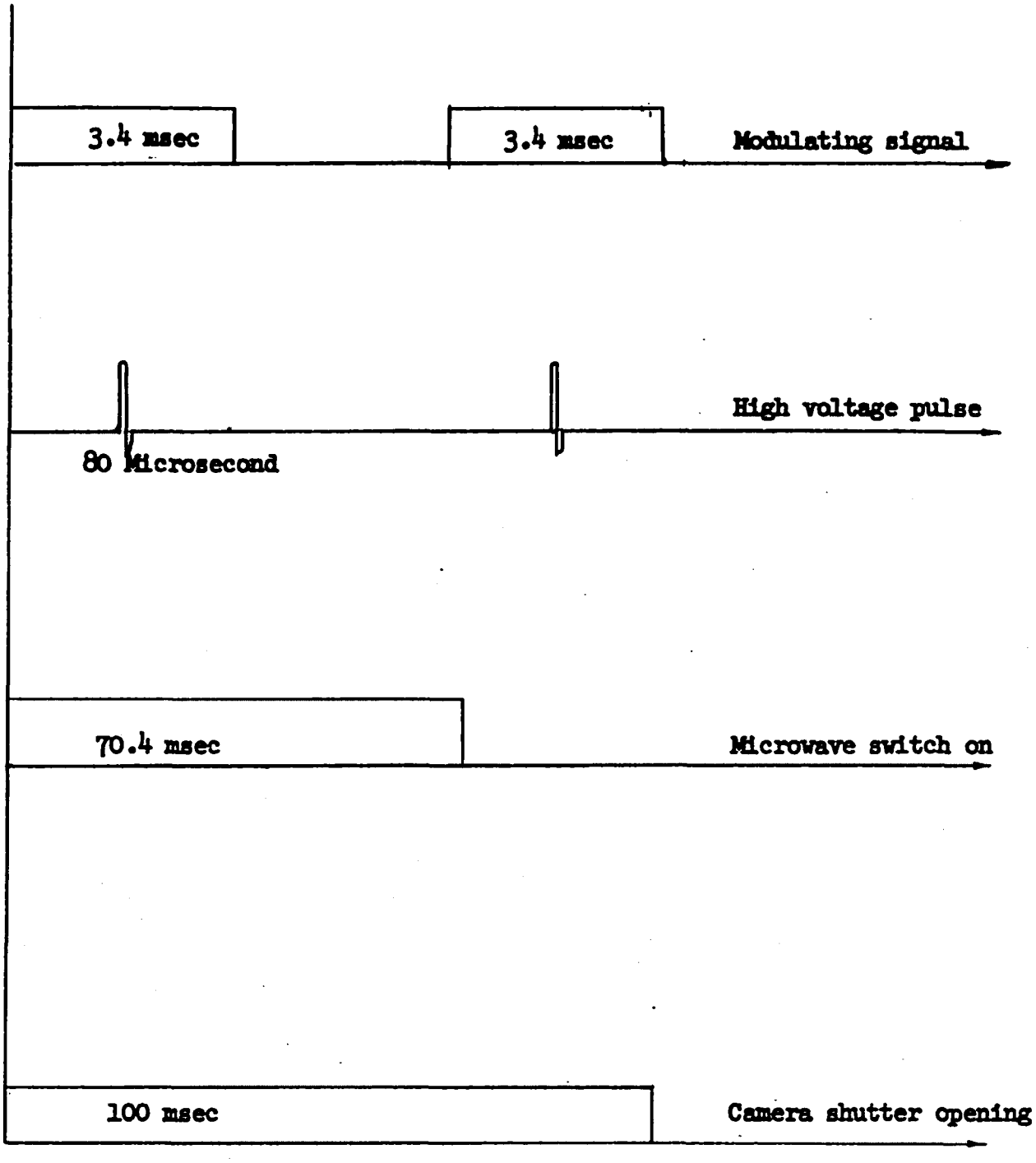

Figure 30 The Relative Waveforms

3. Doppler reflectometer (2, 24, 26)

The reflectometer circuit is shown schematically in Figure 31. The main power input is split into two parts: the horn and the balancing arm. If the reflectometer is balanced, the output of the detector arm is zero, if there is any disturbance in any of the two arms (e.g. the reflection of the medium in front of the horn), then the detector will give an output. At the same time the spectrum analyzer will indicate a phase shift.

The operating steps of Doppler reflectometer

(1) Adjust the cavity of klystron and the shorted end of the detector to obtain a maximum output on both the oscilloscope and SWR meter.

(2) Without ionizing the gas in the tube, obtain the minimum reading on the SWR meter by adjusting the attenuators and phase shifter of the balancing arm. Note, at this moment, the spectrum analyzer SA-84WA should read only the noise pattern.

(3) Disturb the phase shifter or the attenuator to obtain a small output of the detector arm to the SA-84WA spectrum analyzer. Note, this is the klystron operating frequency.

(4) Ionize the gas in the tube by turning on the dc SW of the power supply and the two logic level control power supplies.

(5) Turn on the microwave switch.

(6) After turning on the pulser, the spectrum analyzer should give a phase shift pattern on its screen.

If the phase shift is difficult to distinguish from the original signal, the dispersion SW may set into low, change to maximum sensitivity

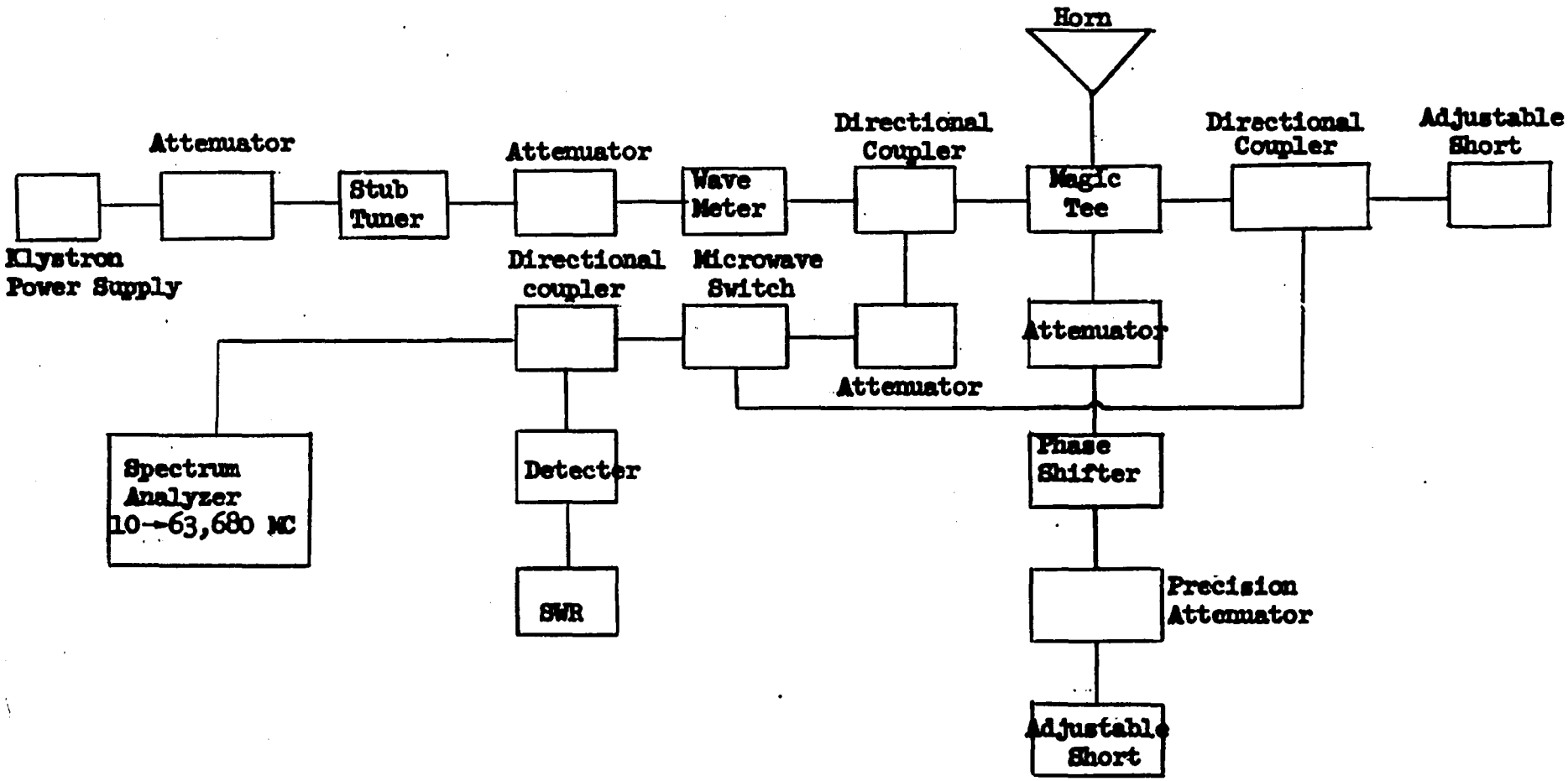

Figure 31 Doppler Reflectometer

which gives the minimum readable frequency of 1 Kc.

4. Vacuum system and ionization tube

The vacuum system includes a Welch 1410 vacuum pump, a vacuum trap and a ionization tube. The minimum pressure of this system is 0.15 mm Hg.

The ionizing tube consists of two Aluminum plates 3.5" in diameter. The bottom plate has a $1\frac{3}{4}$" x $2\frac{1}{4}$" rectangular hole in the center with a microwave horn under it. In order to reduce the noise, the top plate is curved as shown in Figure 32.

5. Spectrum Analyzer (25)

A Polarad SA-84WA spectrum analyzer is used to measured the phase shift.

The detailed operating procedure is enclosed in the Appendix.

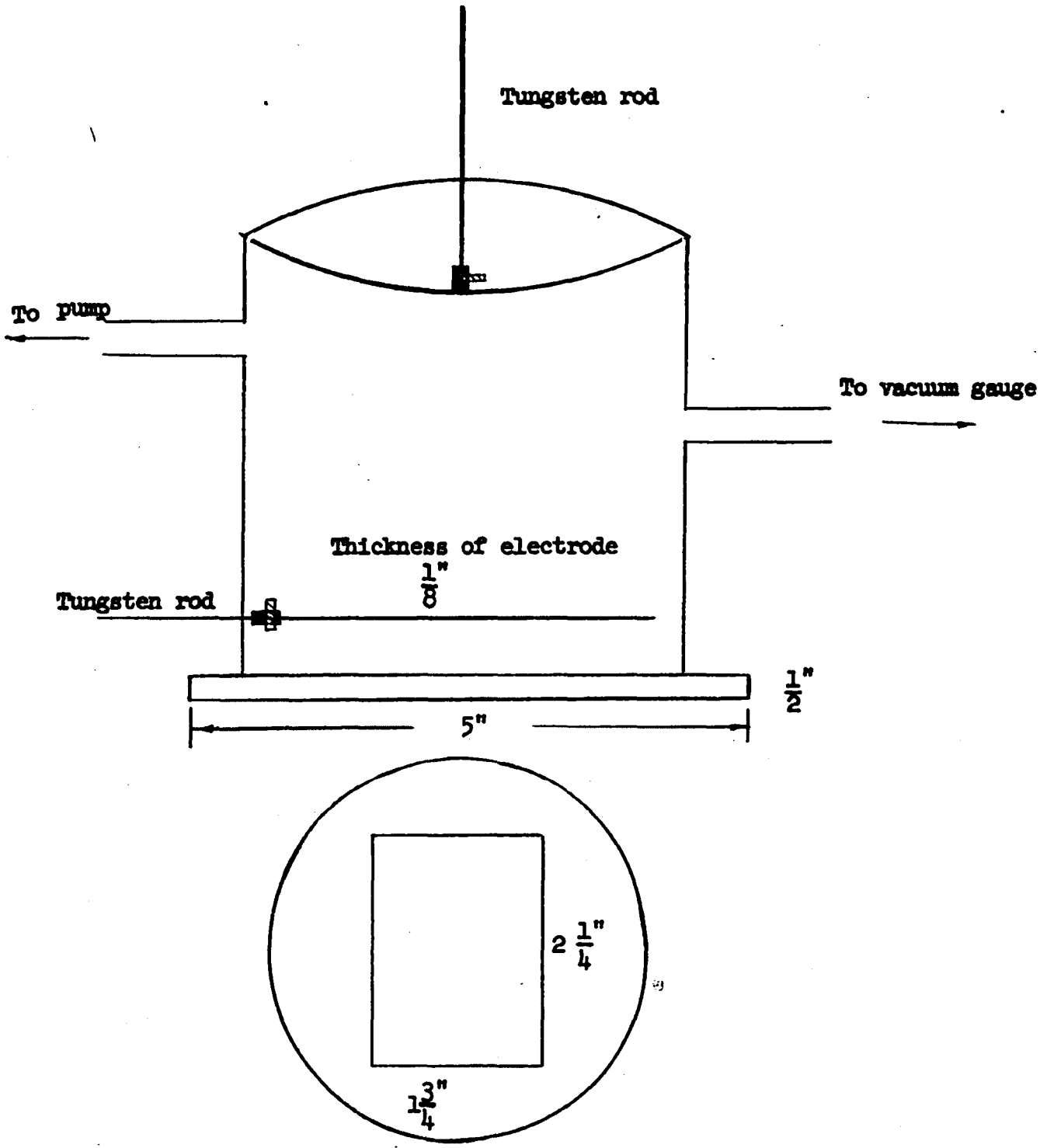

Figure 32 The Ionization Tube

CHAPTER V

RESULTS

Using the special experimental technique developed in this research which was described in Chapter IV, the Doppler frequency shift becomes measurable. The experimental results show the higher the applying frequency, the more the frequency shift. This is in agreement with the theory which is developed in Chapter III.

The operating frequency of klystron (13) is in the range of 26 kmc. It is found that within a range of 33.5 kmc to 36.25 kmc, the klystron will deliver the maximum output of about 50 mw. Selection of frequency of 35 kmc was made for several reasons. Paramount among these was the fact that this frequency is much above the plasma resonant frequency, should a plasma exist in the region between the plates. Previous experiments have shown that the resonant frequency utilizing the equipment at hand (maximum power of 500 watts and one micron Hg. pressure) should be no greater than 8 kmc. As a result, the interaction between the 35 kmc center frequency of the Doppler reflectometer and the medium will be negligible. A second reason is the fact that to get a true picture of the velocity, the region or distance traveled by the ions must be several wavelengths, as compared to the wavelength of the Doppler center frequency. For the 35 kmc wavelength of 8.6 millimeters, this is easily achieved in

the tube utilized in the experiment. A third reason for using 35 kmc is the fact that the noise background is almost negligible and hence, no interaction between the dispersion of frequencies produced by the breakdown phenomena will be recorded on the spectrum analyzer. As a further comment, it was noted that when the Doppler reflectometer was properly tuned, the minimum detectable signal of 90 dbm showed no output with no applied voltage.

During the test run under these conditions, the pressure in the tube was 0.15 mmHg. with air as the operating medium. The use of the Doppler reflectometer in this configuration to permit measure ion front velocity in preignition breakdown currents has been quite successful. The experimental results show that as high voltage (2.1 kv) is applied to the anode of the tube that a shift in the spectral line as shown in Figure 33 occurs. Under the same conditions only with no voltage applied it is easily seen from Figure 34 that no shift in the frequency spectrum has occurred. This same effect has been noted on several different runs and is a very consistant measure of the ion front velocity.

A number of tests were then performed to determine if the measure was actually that of positive ions or perhaps some noise characteristics from the discharge. If the polarity of the voltage pulse to the tube is reversed the Doppler shift should be in a direction opposite to that which previously measured, when the positive ion front was coming toward the Doppler reflectometer horn. This did occur and showed that the Doppler shift was of a higher frequency when the positive ions were propagating away from the horn. A further check to determine whether or not the influence of a plasma in the field of a horn would unbalance the

bridge was made through application of high voltage dc. In this test the tube was allowed to come to a brillant glow and stabilize. In no case did the bridge unbalance, showing that a change in the dielectric properties of the medium had no effect on the Doppler reflectometer balance at plasma resonant frequencies below 8 kmc (23). A further test to determine if the effect of high voltage was disturbing the reflectometer was made by testing voltage application up to, but not including a prebreakdown discharge. This was done by applying voltage pulses but not allowing current to flow during this interval. In no instance did the reflectometer null reading or balance position change. Other precautions taken include cleaning and outgasing of the vacuum system to avoid as nearly as possible a contamination of the surface, although this factor did not seem to be particularly important since this was a gaseous type discharge in which an avalanche did occur, rather than a vacuum discharge in which the purity conditions of the evacuated chamber are very important.

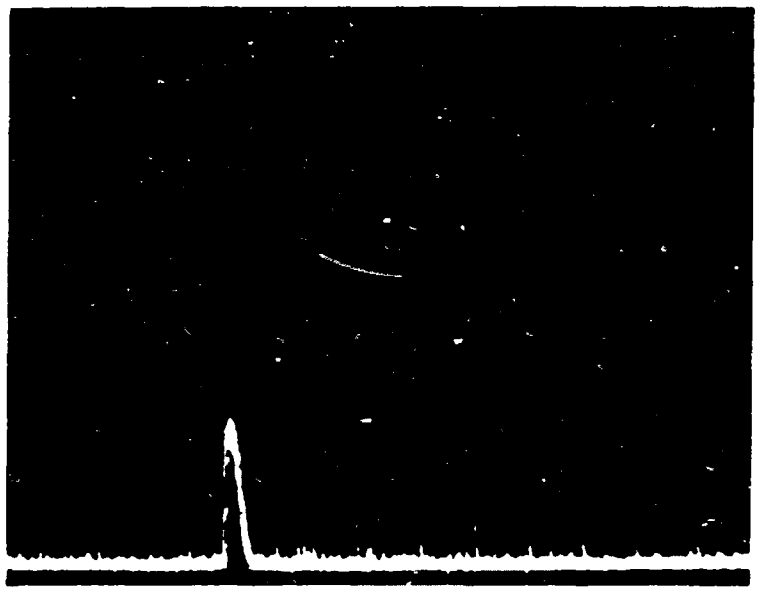

Figure 33 The Frequency Spectrum With High Voltage On (2.1 kv, f=33.55 kmc)

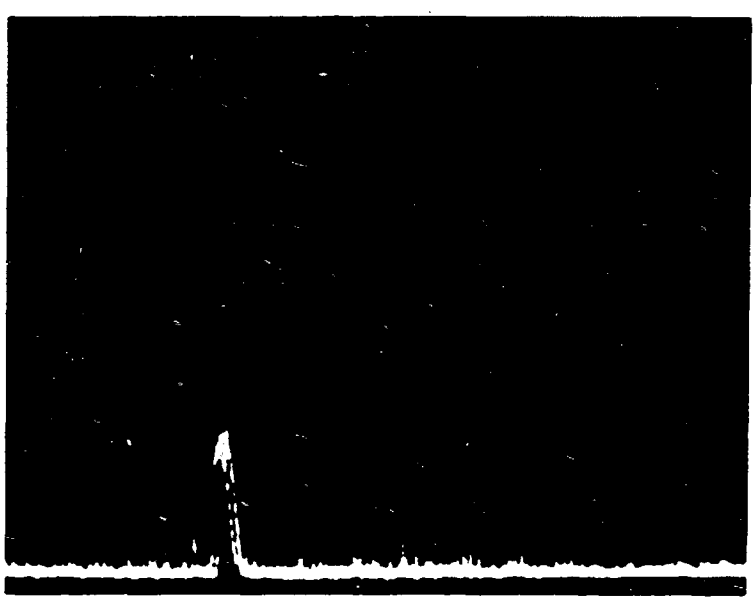

Figure 34 The Frequency Spectrum Without High Voltage On (f=33.55 kmc)

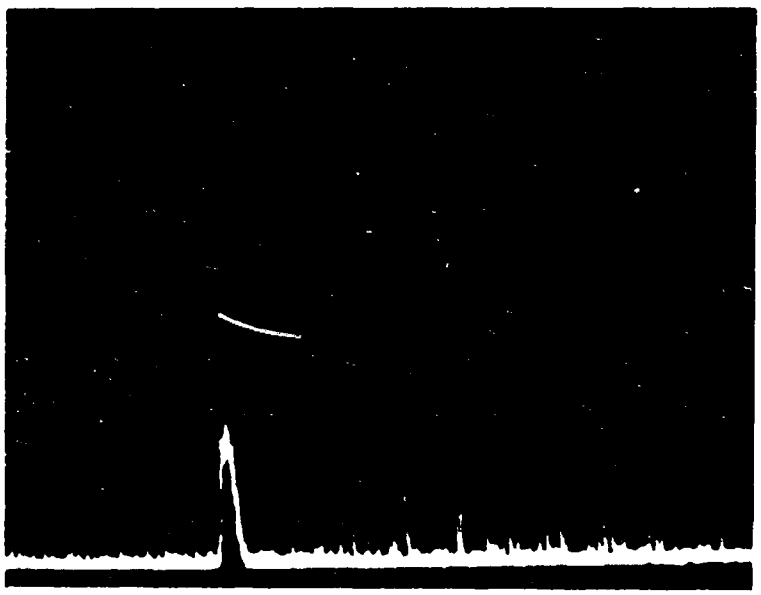

Figure 35 The Frequency Spectrum With High Voltage On (2.1 kv, f=33.75 kmc)

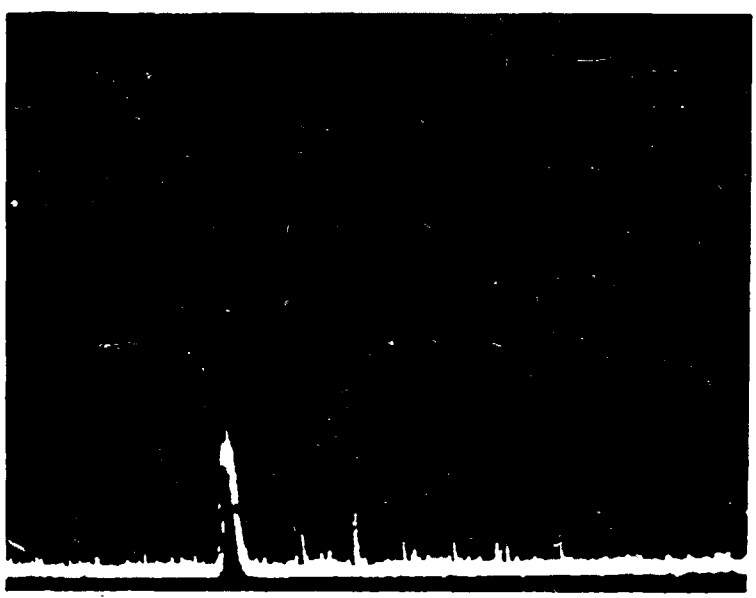

Figure 36 The Frequency Spectrum Without High Voltage On (f=33.75 kmc)

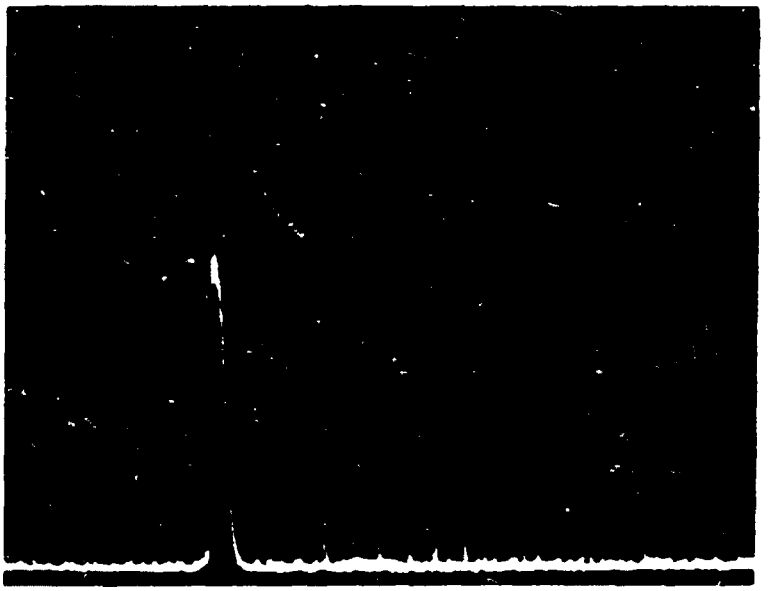

Figure 37 The Frequency Spectrum With High Voltage On (2.1 kv, f=37.5 kmc)

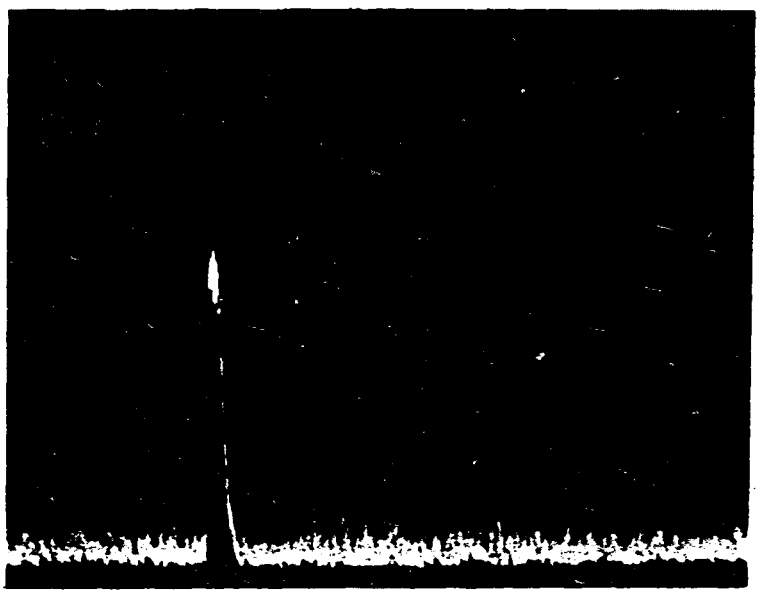

Figure 38 The Frequency Spectrum With High Voltage On (2.1 kv, f=33.25 kmc)

From Figure 33 and 34,

$f = 33.55$ kmc $\qquad \Delta f = \frac{4}{46}$ mc

By assuming that $v \ll c$, then, from equation (3-28),

$$v = \frac{\Delta f \times c}{2f}$$

$$= \frac{\frac{4}{46} \times 3 \times 10^8}{2 \times 33.55 \times 10^3}$$

$$= \frac{3 \times 10^8}{23 \times 33.55 \times 10^3}$$

$$= \frac{3 \times 10^5}{771.65}$$

$$= 0.0038 \times 10^5$$

$$= 0.38 \times 10^3 \text{ m/sec.}$$

From Figure 35 and 36,

$f = 33.75$ kmc $\qquad \Delta f = \frac{4.5}{47}$ mc

$v = 0.43 \times 10^3$ m/sec.

From Figure 37,

$f = 37.5$ kmc $\qquad \Delta f = \frac{6}{51}$ mc

$v = 0.48 \times 10^3$ m/sec.

From Figure 38,

$f = 33.25$ kmc $\qquad \Delta f = \frac{4}{52}$ mc

$v = 0.36 \times 10^3$ m/sec.

From the calculated results, the velocity of ions in electrical prebreakdown is approximately of the order of 10^3 m/sec.

The volt-ampere characteristics are shown in Figure 39, 41, 43, 45, 47 and 48.

Figure 39 and 40 show the minimum breakdown voltage to be 600 v. Under these conditions, the pressure in the tube was 0.15 mm Hg. with air as the operating medium.

Table 3 gives the time lag against the applied voltage to the tube.

Table 3 Time Lag Against The Overvoltage Applied

Overvoltage (percentage)	350	300	250	160
Time Lag (microseconds)	0.65	1.2	1.5	2.0

It is found that the higher the overshoot voltage applied the less time lag will be. This is in good agreement with the results of other workers such as Morgan (21).

Figure 39 The Minimum Breakdown Voltage (200 v/cm)

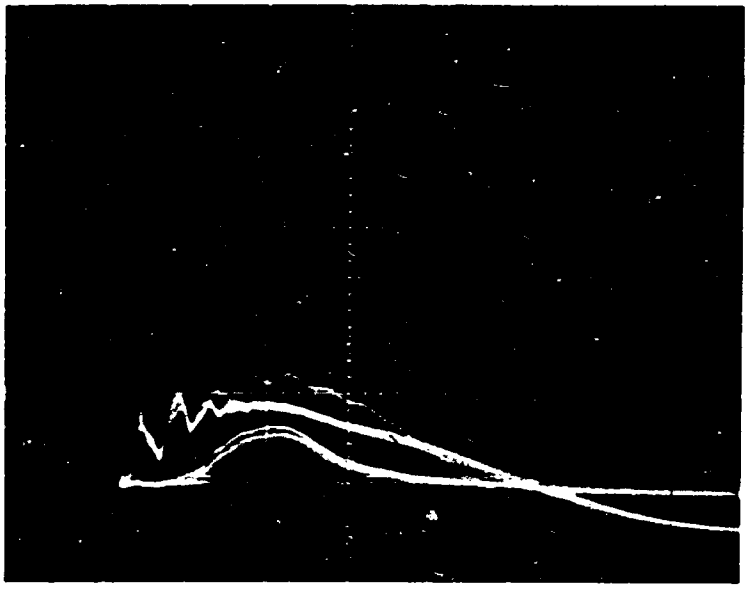

Figure 40 The Voltage and Current Traces
Voltage = 0.5 kv/cm
Current = 10 ma/cm
Time = 20 μs/cm

Figure 41 Volt-ampere Curve
Voltage = 0.2 kv/cm
Current = 5 ma/cm

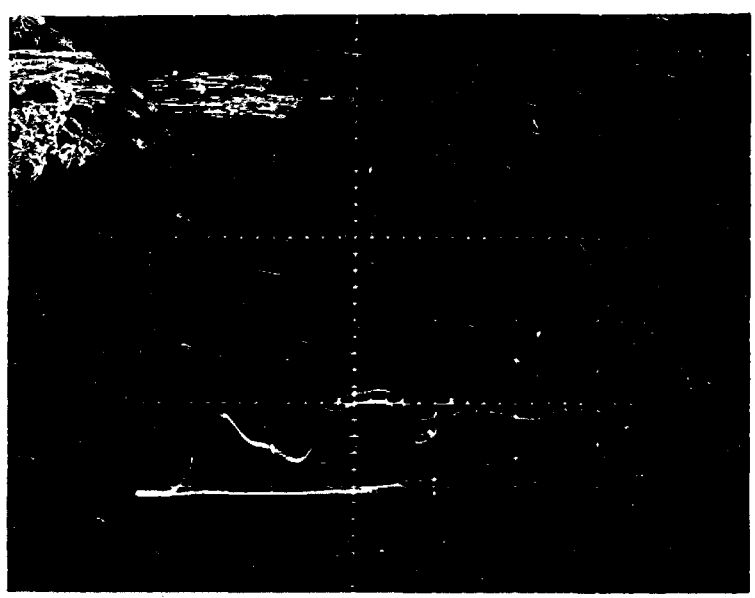

Figure 42 Volt-ampere Curve (Expended Traces)
Voltage = 0.5 kv/cm
Current = 10 ma/cm
Time = 5 μs/cm

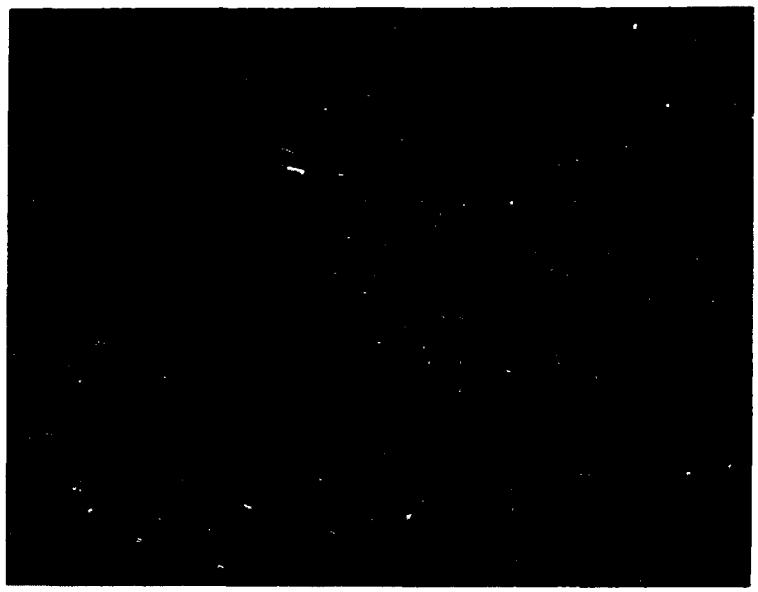

Figure 43 Voltage-ampere Curve
Voltage = 0.5 kv/cm
Current = 20 ma/cm

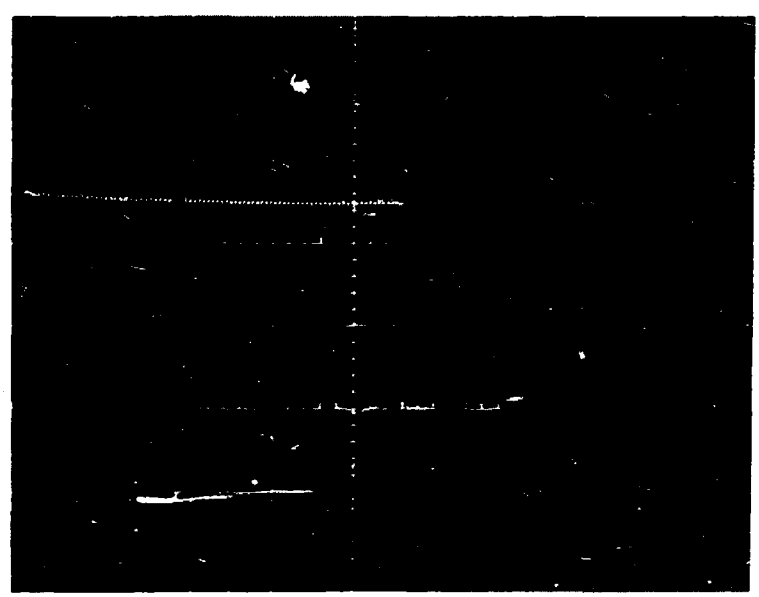

Figure 44 Voltage-ampere Curve (Expended Traces)
Voltage = 0.5 kv/cm
Current = 10 ma/cm
Time = 5 μs/cm

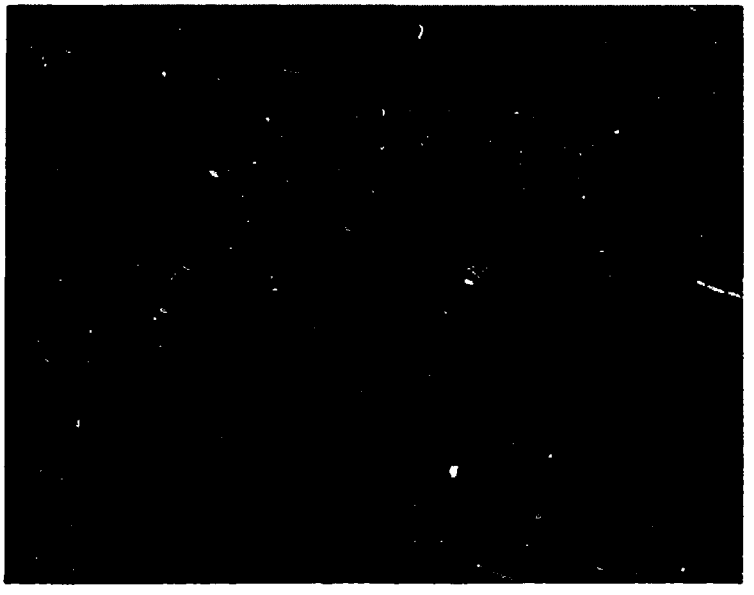

Figure 45 Volt-ampere Curve
Voltage = 0.5 kv/cm
Current = 20 ma/cm

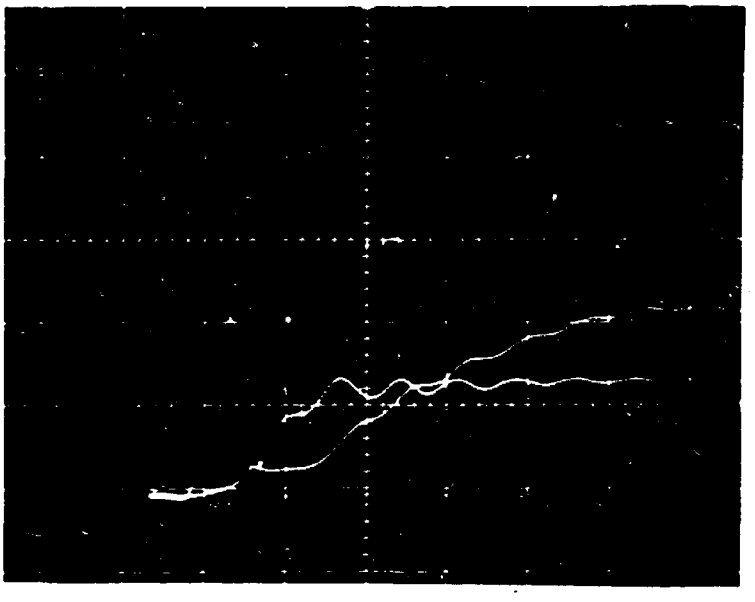

Figure 46 Volt-ampere Curve (Expended Traces)
Voltage = 0.5 kv/cm
Current = 10 ma/cm
Time = 5 μs/cm

Figure 47 Volt-ampere Curve
Voltage = 0.5 kv/cm
Current = 10 ma/cm

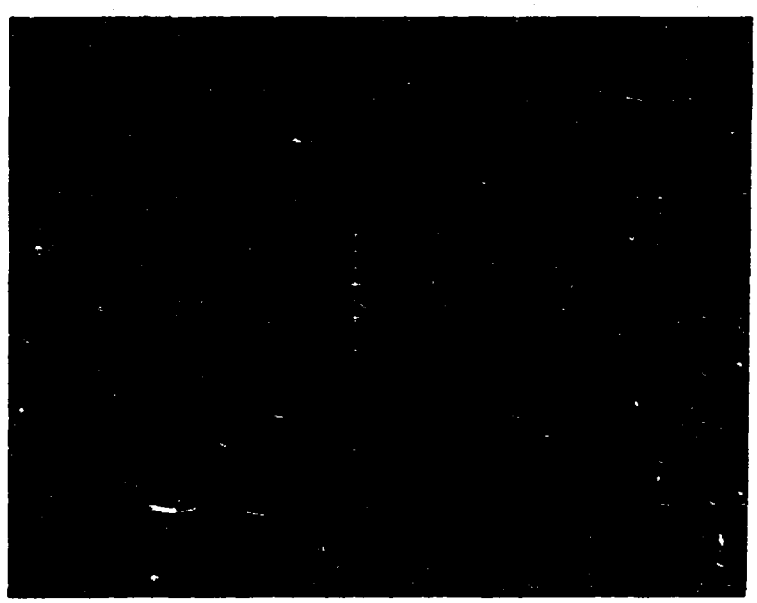

Figure 48 Volt-ampere Curve (Expended Traces)
Voltage = 1 kv/cm
Current = 10 ma/cm
Time = 5 μs/cm

CHAPTER VI

CONCLUSIONS AND RECOMMENDATIONS

The velocity of positive ions in preignition breakdown has been an estimated value for years (20). It has never been successfully measured. The difficulties are due to the complex characteristic of the discharge tube. The special experimental technique developed in this research makes this measurement possible.

The experimental results show the following: For a carrier frequency of 33.55 kmc, the Doppler shift was found to be 4/46 megacycles yielding a velocity of 0.38×10^3 meters per second as shown in Figure 33. From Figure 35 with a center frequency of 33.75 kmc and Doppler shift of 4.5/47 megacycles, the velocity was found to be 0.43×10^3 meters per second, and in Figure 37 where the carrier frequency was 37.5 kmc, the Doppler shift was 6/51 megacycles with a corresponding positive ion velocity of 0.48×10^3 meters per second. These results compare very favorably to those predicted by many researchers (38, 21) as being necessary for the electrical breakdown of gases under high voltage. These results show that the velocity of positive ions in the prebreakdown currents has been determined, a value which has never been measured directly.

The theoretical and experimental work performed in this research have led to many interesting possibilities in the field of gaseous discharges. These related problems are presented as recommendations of this dissertation:

1. With a slight modification of equation (3-21), a relativistic (22, 41, 34) Doppler frequency shift equation can be obtained as,

$$\Delta f = \frac{2fv}{c}\left(1 - \frac{v^2}{c^2}\right)^{-1/2}\left(1 + \frac{1}{2}\Delta\epsilon_r + \ldots\right) \qquad (6\text{-}1)$$

where

$$\Delta\epsilon_r = \frac{-f_p^2}{f^2}$$

f_p is the plasma frequency

f is the propagating wave frequency

$$\Delta f = \frac{2fv}{c}\left(1 - \frac{v^2}{c^2}\right)^{-1/2}\left(1 - \frac{1}{2}\frac{f_p^2}{f^2} \ldots\ldots\right) \qquad (6\text{-}2)$$

Equation (6-1) shows that the plasma frequency is a function of particle speed which has never been measured.

2. In 1959, Hibberd and Thomas (14, 28) tried to calculate the Doppler shift of SPUTNIK I, and gave the following:

$$\Delta f = \frac{f_o v \mu_s}{c}\left(\cos\alpha \sin\psi_s - \cos\beta \cos\psi_s\right) \qquad (6\text{-}3)$$

where α and β are the directional cosines to the X and Y axes. The refractive index at the satellite is denoted by μ_s; until 1964, Titheridge (35) used the same μ to be the phase refractive index and gave the Doppler shift, as

$$\frac{\Delta f}{f} = -\frac{v}{c}\mu\cos\alpha \qquad (6\text{-}4)$$

Generally speaking μ is not a constant. In an inhomogeneous medium, according to (6-1)

$$\mu = \left(1 + \frac{1}{2}\Delta\epsilon_r\right)$$

$$= 1 - \frac{f_p^2}{f^2}$$

Hence, by using the same technique developed in this research, the Doppler frequency shift of satellite can be obtained.

The following areas are noted as having rather severe equipment limitations and very definitely in need of further development.

1. The time lag is found to be inversly proportional to the applied overshoot voltage, but due to the poor waveshape of the pulser an ideal rectangular pulse is not obtained and no further prediction can be made from the present data. The waveform of the pulser can be improved by rewinding the transformer or using thyratrons instead of [illegible] to be the switching devices.

2. The klystron frequency is dependent on the operating voltages and the ambient temperature, the drift of the klystron frequency should be stabilized.

The further work to develop the technique under other operating condition and to refine the technique are recommended as follow:

1. Bring voltage to just under breakdown and irradiate with α and check breakdown speed.

2. Investigate the effect of different gases in electrical prebreakdown.

3. Investigate the effect of electrode material and configuration related to the ion velocity in the electrical prebreakdown.

4. Investigate the effect of pressure, the spacing between the electrodes, and the purity of medium related to the ion velocity in the electrical prebreakdown.

BIBLOGRAPHY

1. Anderson, L. M. and M. L. Goldstein, "Interaction of Electromagnetics Waves of Radio-frequency in Isolthermal Plasma" Phys. Rev., Vol. 100, (1955) p. 1037.

2. Anderson, J. M. "Cavity Method Suitable for Measurement of High Electron Densities in Plasma" Rev. Sci. Instrum., Vol. 32 (1961) p. 975.

3. Bergmann, P.G., "Introduction to the Theory of Relativity" Prentice Hall Inc., 1942.

4. Birkltoff, G. D., Relativity and Modern Phusics, Cambridge Harvard University Press, 1923.

5. Brown, S. C., "The Interaction of Microwaves with Gasdischarge plasma" IRE Tran. M. T.T., Vol. 7,(1959) p. 69.

6. Buser, R. and W. Buser, "Determination of Plasma Properties of Free Space Microwave Techniques" J. Appl. Phys. Vol. 33,(1962) p. 2275.

7. Drummond, J. E. Plasma Physics, McGraw Hill Company, 1961.

8. Flugge, S.,Handbuch der Physik, Springer-Verlag, 1956.

9. Francis Gordon, Ionization in Gas, New York Academic Press Inc., 1960.

10. G.E. Transistor Manual, Edition 6, 1962.

11. G.E. SCR Manual, 2nd Edition, 1962.

12. Doldstein, M. L., "Magneto-optics of an Electron Gas with Guided Microwaves" Phys. Rev., Vol. 82 (1951), p. 956.

13. Harrison, A. E., Klystron Tube, McGraw Hill Book Company, 1949.

14. Hibberd, F. H. and J. A. Thoma, "The Determination of the Electron Distribution in the Upper Ion Sphere From Satellite Doppler Observation" J. Atom. and Terr. Phys., Vol. 17 (1959).

15. Strauss, L., Wave Generation and Shaping, McGraw Hill Book Company, 1960.

16. Llewllyn-Jones, F. Ionization and Breakdown in Gases, Methuen & CO. LTD., London, 1958

17. Loeb, L. B., Basic Processes of Gaseous Electronics, Berkeley, University of California Press, 1955.

18. Mapham, N., "Using SCR Successfully with Steep Current Wave Form" G.E., 1962.

19. Marcuvitz, N. Waveguide Handbook, McGraw Hill Book Company, 1951.

20. Meek, J. M. and J.D. Craggs, Electrical Breakdown of Gases, Oxford Clarendon Press, 1953.

21. Morgan, C. G.,Conference on Ionized Gases at Birmingham University, App. Sci. Rev., Vol. B 5, 1955.

22. Ney, E. P., Electromagnetism and Relativity, Harper and Row Publishers, 1962.

23. Palmer, J. D. Private Communication.

24. Handbook of Microwave Measurement, Vol. 1 and 2, Polytechnique Institute of Brooklyn, 1954.

25. Polarad Microwave Spectrum Analyzer, Polarad Electronic Instruments, 1963.

26. Postma, A. J. and Terlouw, J. C.,"Calculation and Measurements on an x-band Microwave Interferometer" Plasma Phys.(J. Nucl. Eng. Part C) Vol. 5,(1963) p. 37.

27. Reich, H. J., P. F. Ordung, H. L. Krauss, and J. G. Skalnik, Microwave Theory and Techniques, D. Van Nostrand Co. Inc., 1953.

28. Ryerson, J. L., "Possive Satellite Communication" Proc. IRE, Vol. 48 (1960), p. 617.

29. Sanders, F. H., "The Value of the Townsend Coefficient for Ionization by Collision at Large Plate Distance and Near Atmosphere Pressure" Phys. Rev., Vol. 41 (1932) p. 667.

30. Schade, R., "Uber die Aufbauzeit Einer Glimmentladung" Z. Physik, Vol. 104 (1937) p. 487.

31. Schumann, W. O. Elektrische Durchbruchfeldstarke in Gasen, Berlin, Spring, 1923.

32. Schwartz, M, Information Transmission Modulation and Noise, McGraw Hill Book Company, 1959.

33. Steinmetz, C. P., Four Lectures on Relativity and Space, McGraw Hill Book Company, 1923.

34. Stephenson, G. and C. W. Kilmister, Special Relativity for Physics., London's Green & Co., London, 1958.

35. Titheridge, J. E., "The Reflection of Satellite Signals I and II" J. of Atm. and Terr. Phys., Vol. 26, no. 2, February, 1964.

36. Townsend, J. S., Electricity in Gases, Oxford at the Clarendon Press, 1915.

37. Townsend, J. S., The Theory of Ionization of Gases by Collision, London Constable and Co. LTD, 1910.

38. Vernerin, L. J., "Electron Recombination and Collision Cross-Section Measurement in Hydrogen" Phys.Rev., Vol. 84 (1951), p. 563.

39. Von Engel, A., Ionized Gases, Oxford at the Clarendon Press, 1955.

40. Wharton, C. B. and D. M. Slager, "Microwave Determination of Plasma Density Profiles" J. Appl. Phys., Vol. 31, p. 428.

41. Whitehead, A. N., The Principle of Relativity with Application to Physical Science, Cambridge at the University Press, 1922.

42. Whitmer, R. F., "Microwave Studies of Electron Loss Processes in Gaseous Discharges" Phys. Rev. Vol. 104 (1956), p. 572.

43. Wyckoff, R. W. G., The Structure of Crystals, The Chemical Catalog Co., 2nd ed., New York (1935).

44. Zeleny, J., "The Mechanism of the Electric Spark" J. Appl. Phys., Vol. 13 (1942), p. 444.

REFERENCES NOT SPECIFICALLY NOTED IN THE TEXT

Allis, W. P., "Handbuch Der Physik", Vol. 21, Heidelberg, Springer, 1956.

Baraff, G. A. and Buchsbaum, S. J., "Anistropic Electron Distribution and the d.c. and Microwave Avalanche Breakdown in Hydrogen", Phys. Rev. V. 130, p. 1007, 1963.

Baranger, M. and B, Mozer, "Electrical Field Distributions in an Ionized Gas" Phys. Rev., Vol. 155, P. 521, 1959.

Bevc, V. and T. E. Everhagt, "Fast wave Propagation in Plasma Filled Waveguide" J. Electron. Contr., V. 13, p. 185, 1962.

Bhattacharya, H., "Amplitude and Phase Spectrum of Radio Atmospherics" J. of Atm. and Terr. Phys., V. 25, p. 445, 1963.

Blair, D. T. A., "Prebreakdown Phenomena in Uniform Field" Proc. Phys. Soc., 75, p. 729, 1960.

Blevin, H. "Electrical Breakdown of Gases in the Presence of a Transvers Magnetic Field" CIM-R-10, 1961.

Brown, S. C. "Propagation of Electromagnetic Wave in Plasma" Phys. Today, Vol. 15, p. 70, 1962.

Bryant, G. H. "Propagation in a Waveguide Field Non-uniformly With Plasma" J. Electron. Contr., Vol. 12, p. 297, 1962.

Crawford, F. W. "A Microwave Method for the Study of Steady and Fluctuating Plasma number Density" J. Appl. Phys., Vol. 34, p. 2186, 1963.

Croom, D. L. "The Frequency Spectra and Attenuation of Atmospherics in the Range 1-15 kc/sec." J. of Atm. and Terr. Phys. Vol. 26, p. 1015, 1964.

Dellis, A. N. and Weaver, J. M. "Measurement of a High Reflective index for Transmission of 3-cm Microwave Through a Plasma" Nature, London, Vol. 193, p. 1274, 1962.

Dubois, D. F. "Propagation of Electromagnetic Wave in Plasma" Phys. Rev., Vol. 129, p. 2376, 1963.

Dutton, J. "Electrical Breakdown of Gases, Ionization Growth in Air at High-pressure" Proc. Phys. Soc., Vol. 78, p. 569, 1961.

Dyson, J. "Interferometric Measurement of Electron Density in Sceptre IV" Nature, London, Vol. 195, p. 1291, 1962.

Ericson, M. "Containment of Plasma by High Frequency Electric Field" J. Appl. Phys. Vol. 33, p. 2429, 1962.

Flavell, R. G. and Lane, J. A. "The Application of Potential Refractive Index in Tropospheric Wave Propagation" J. of Atm. and Terr. Phys., Vol. 24, p. 47, 1962.

Flock, W. L. and Elliott, R. S. "The Radiation Pattern of a Microwave Horn and a Plasma Layer", Inst. Radio Engr., Ap-10, p. 65, 1962.

Forman, R. "Electrical Conduction and Breakdown in High Pressure Rare Gases" Phys. Rev. Letter, Vol. 6, p. 594, 1961.

Grossdopt, J. "Aircraft Reflection at V. H. F. and U. H. F." NBS Tech. Report No. 5565, 1962.

Harding, G. N. and Robert, V. "Proceedings of the 5th International Conference on Ion Phenomena in Gas" p. 1977, 1961.

Hoffman, W. C. "A Possible Mechanism for Radiation and Reflection from Ionized Gas Clouds" Proc. IRE, Vol. 47, p. 1274, 1959.

Kelly, D. C. "General Theory of the Microwave Conductivity of a Plasma in a Magnetic Field" Bull Amer. Phys. Soc. Ser. II, Vol. 4, p. 318, 1959.

Kurilko, V. I. "Reflection of Electromagnetic Wave from a Plasma Moving in a Slow Waveguide" Sov. Phys. Tech. Phys., Vol. 6, p. 655, 1962.

Lisitano, G. "Microwave Interferometer With 1 US Break" ILL/2/15, 1962.

Macdonald, A. D. "Microwave Breakdown in Air" Phys. Rev., Vol. 130, p. 1841, 1963.

Mariner, P. F. "Introduction to Microwave practice" London,Heywood & Co. LTD 1961.

Miyoshi, Y. "Development of Space Charge and Growth of Ionization in the Transient Townsend Discharge" Phys. Rev. Vol. 117, p. 335, 1960.

Mitsuk, V. E. "The Electric Field in a Microwave Plasma as a Function of Time"zh. eksp. teor. Fiz., Vol. 36, p. 1603, 1959.

Northover, F. H. "The Propagation of Electromagnetic Waves in Ionized Gases" J. Atm. Terr. Phys., Vol. 17, p. 158, 170.

Purson, K. B. "Limitations of the Microwave Cavity Method of Measuring Electron Densities in a Plasma" Phys. Rev. Vol. 106, p. 191, 1957.

Baylor, R. L. and Kerakovity, S. B. "A Plasma Microwave Engergy Detector" Proc. IRE, p. 1901, 1961.

Sakamoto, Y. and Miyoshi, S. "Measurement of Electron Temperature of Plasma by Microwave Method" Japan J. Appl. Phys. p. 245, 1963.

Sodmsky K. F. "Microwave Measurements of Moving Striation in d.c. Glow Discharge" J. Appl. Phys. Vol. 34, p. 1860, 1963.

Smallin, L. D. and Chorney, P. "Properties of ion Field Waveguide" IRE, Vol. 46, p. 360, 1958.

Tornebohn, H. "A Logical Analysis of the Theory of Relativity" Almquist and Wiksell Stockhom, Sweden, 1952.

Tsukishima, T. and Taked, S. "Microwave Reflection by Magnetic Plasma" J. Phys. Soc., Japan Vol. 18, p. 1056, 1963.

Vermeer, A. "Microwave Doppler Shift Measurements on the Plasma of Arc Discharge" Phys. Letter, Vol. 3, p. 25. 1962.

Wagmouth, J. P. "Pulse Technique for Probe Measurements in Gas Discharge" J. Appl. Phys., Vol. 30, p. 1404, 1959.

APPENDIX

The operating steps of spectrum analyzer

1. Adjust the horizontal vertical gain position. Focus and brightness controls to obtain a sharp base line on the CRT screen.

2. Adjust the vertical position control to locate the baseline on the CRT screen directly below the horizontal line etched with vertical marks on the CRT graticule.

3. Set the dispersion SW to the high position.

4. Rotate the dispersion control fully clockwise.

5. Off all IF attenuator DB switch.

6. Set the LOG-FILTER-LIN switch in LIN.

7. Rotate bandwidth control maximum clockwise.

8. Rotate the vertical gain control to obtain approximately 1/8" of noise on CRT screen.

9. Rotate the marker amplitude control beyond the off position (clockwise).

10. Rotate the frequency difference MCS turning control to line up the 0 mark. This operation places the marker pip at the electrical center of the display.

11. Rotate the center frequency control to position the marker pip at the physical center of the CRT display.

12. Set the SYNC SELECTOR to the off position.

13. Set the sweep speed control to 8.

14. Rotate the marker amplitude control to set the height of the marker pip at approximately three inches.

15. Set the bandselect switch to the frequency range where the klystron is operating, then by turning the dial from left to right; two signals will appear in the CRT screen. Note, when the dial moves from left to right, if the spectrum signal moves also left to right, it indicates that the spectrum is the image of the signal, and if the dial moves from left to right the spectrum moves from right to left, then the spectrum is the signal.